SEQUENCE STRATIGRAPHY AND CHEMOSTRATIGRAPHY OF AN INCISED VALLEY FILL WITHIN THE CRETACEOUS BLACKHAWK FORMATION, BOOK CLIFFS, UTAH

By

Christine Frasca Cornwell

B.S., Virginia Polytechnic Institute and State University, 2010

Submitted to the graduate degree program in Geology and the Graduate Faculty of the University of Kansas in partial fulfillment of the requirements for the degree of Master of Science.

_____

Co-Chairperson Diane Kamola

_____

Co-Chairperson Luis González

_____

Michael H. Taylor

Date Defended: November 15, 2012

The Thesis Committee for Christine Frasca Cornwell

certifies that this is the approved version of the following thesis:

SEQUENCE STRATIGRAPHY AND CHEMOSTRATIGRAPHY OF AN INCISED VALLEY
FILL WITHIN THE CRETACEOUS BLACKHAWK FORMATION, BOOK CLIFFS, UTAH

_____

Co-Chairperson Diane Kamola

_____

Co-Chairperson Luis González

Date approved: December 12, 2012

ABSTRACT

A better constraint on the timing and depositional development of the incised valley fill (IVF) of the Desert Member of the upper Cretaceous Blackhawk Formation was needed to help understand the development of incised valley fills. Paleosol analysis and chemostratigraphy were used to refine the previously published sequence stratigraphic interpretation of this valley fill. This study is a proof of concept project that tested the ability to use $\delta^{13}C_{org}$ chemostratigraphy with sequence stratigraphy to refine the stages of an IVF at the parasequence level.

The incised valley fill within the Desert Member of the Blackhawk Formation in Tuscher Canyon, Utah was measured and described for the following reasons: paleosol facies interpretations at the detailed parasequence-scale sequence stratigraphy, and $\delta^{13}C_{org}$ chemostratigraphy. From field observations, three moderately developed paleo-Histosols, three weakly developed paleo-Inceptisols, and four very weakly developed paleo-Entisols were described within the study area. Based on the $\delta^{13}C$ profiles from the measured sections, eight chemostratigraphic events were characterized. Using the analyses from the facies and paleosols, five parasequence boundaries were selected within the IVF of the Desert Member.

The IVF was divided into nine stages of fill using the parasequence stratigraphy and chemostratigraphy. Stages of valley fill are defined by changes in base level. A minimum-average-age was determined for five stages (numbers 3, 4, 5, 6, and 8) based on paleosol maturity within each stage. A total minimum-average-age for pedogenesis within the IVF is 32,000 years. The paleoclimate of the Desert Member is determined from the paleosol facies to have been humid.

Chemostratigraphy, sequence stratigraphy, and detailed paleosol interpretations are used to help refine the depositional history of an IVF. A greater understanding of the depositional history of the IVF allows for greater resolution of lateral and vertical variability of facies within the valley fill.

ACKNOWLEDGEMENTS

TABLE OF CONTENTS

INTRODUCTION

Incised valley fills (IVFs) have been studied extensively due to their importance in sequence stratigraphy and because they are commonly major hydrocarbon reservoirs (Atchley et al., 2004; Bridge and Leeder, 1979; Bridge and Tye, 2000; Miall, 1996; Van Wagoner, 1995). Understanding the development and timing of valley fill events has been challenging. Incised valley fill stages at the parasequence scale are laterally discontinuous and have complex geometries that make outcrop studies complicated. The term "stage" is used to refer to a single event or group of related events that contribute to the development of the incised valley. Stage events include discrete fill events bounded by changes in base level marked by parasequence boundaries or sequence boundaries and major events within an IVF such as the formation of sequence boundaries. Further, how allogeneic factors such as paleoclimate, tectonics, and eustasy affect valley fill has been difficult to tease apart (Miall, 1996).

Early work on IVFs focused on the alluvial channel-fill sandstones because the channel-fill sandstones provide the best exposures and are the main reservoir bodies in these systems (Bown and Kraus, 1987). Overbank deposits with paleosols were studied to understand IVF architecture and stages of incised valley fill (Atchley et al., 2004; Bown and Kraus, 1987; Bridge and Leeder, 1979; Cleveland et al., 2007; Wright and Marriott, 1993). Chemostratigraphy within IVFs has also been used to help resolve fill architecture and for correlation (Hildred et al., 2010). Some IVFs, such as those in the Cretaceous Blackhawk Formation of the Book Cliffs, have been studied extensively but lack detailed work on paleosols and still pose questions on stages of fill. Further, there has been no published work using chemostratigraphy in the Blackhawk Formation. Previous work such as Van Wagoner's (1995) seminal work on the sequence stratigraphy and

1

facies architecture of the Desert Member of the Blackhawk Formation and the overlying Castlegate Sandstone in the Book Cliffs, focused on the regional sequence stratigraphy.

This study seeks to address the problem of better constraining the timing of and depositional development of IVFs through a detailed case study of the IVF within the Desert Member of the Blackhawk Formation. This was accomplished by combining a detailed sequence stratigraphic framework with chemostratigraphy of the IVF. Emphasis was placed on the paleosols in the upper part of the IVF. Using sequence stratigraphy and $\delta^{13}C_{org}$ chemostratigraphy for correlations provides stage-by-stage development of the IVF at the parasequence level and adds to a better understanding of the lateral continuity of depositional units. Previous chemostratigraphy work in terrestrial systems has not focused on correlation of chemostratigraphic events at the parasequence scale. This study is a proof of concept project on using chemostratigraphy to correlate, define, and constrain the stages of valley fill at the parasequence level.

The IVF of the Desert Member of the Blackhawk Formation was chosen because of excellent exposures and because the regional sequence stratigraphic framework has been defined (Van Wagoner, 1995). Because of the excellent field expression in a sinuous canyon, the Desert Member is exposed at several different angles. Exposures contain several well preserved paleosols with overbank deposits, tidally influenced fluvial channels, and fluvial strata. Paleosols within the highstand systems tract of the Sunnyside Member of the Blackhawk Formation have been studied previously (Davies et al., 2005), however no work has been published on the paleosols within lowstand systems tracts. Regional work has noted the occurrence of paleosols, but lacks detail about their characteristics (Hoffmeister, 2011; Scheppy, 2000; Van Wagoner, 1995).

Paleosols can be a useful tool for developing the stages of an IVF. They are laterally extensive compared to the fluvial deposits and are very useful for correlation (Wright and Marriott, 1993). Furthermore, paleosols represent a period of known subaerial exposure that persisted long enough for pedogenesis to occur (Retallack, 1998): soils represent periods of depositional hiatuses at those depositional locations in a fluvial system (Bown and Kraus, 1987). Because paleosols represent periods of known subaerial exposure, the top of each paleosol is a parasequence boundary (Van Wagoner et al., 1988). Depending on the type of paleosol, each paleosol could represent thousands to tens of thousands of years (Bown and Kraus, 1987). Paleosols are well suited for isotopic analysis from soil carbonates and abundant organic carbon material. Paleosols have direct contact with atmospheric gasses such as CO_2 which mix directly through infusion into the soil and can be recorded through isotopic ratios.

Chemostratigraphy

Chemostratigraphic analysis involves the correlation of stable isotopic values in strata by using stable isotope ratios such as $^{13}C/^{12}C$ and $^{18}O/^{16}O$ in carbonates or organic matter. This study used $\delta^{13}C_{org}$ because of the prevalence of organic matter within the IVF and the lack of pedogenic carbonates. Correlation using chemostratigraphy is done by matching unique excursions and patterns in the data with respect to the measured stratigraphy. These excursions are often called events, because they reflect a distinct temporally constrained perturbation of the global carbon cycle. The events are coeval regardless of facies because at geologic time scales, $\delta^{13}C$ of atmospheric CO_2 can be treated as responding instantaneously to carbon cycle perturbations that affect atmospheric CO_2 isotopic composition. These events and patterns may last from a few thousand years to several million years. The unique events and patterns can pinpoint time equivalent points in stratigraphic successions or bracket strata of coeval time.

Quantitative chemostratigraphic analysis requires some basic temporal control of the units being correlated (e.g. biostratigraphy, radiometric dates, thermochronology) and the existence of master chemostratigraphic profiles generated from a section with continuous deposition and good temporal control. In terrestrial sequences, chemostratigraphic analysis using organic matter relies on the fact that plant organic matter samples atmospheric CO_2 on a continuous basis.

Sequence stratigraphy utilizes coeval surfaces, such as parasequence boundaries, for correlation. These are interpreted based on facies and stratal relationships, as defined by Van Wagoner et al. (1988). In chemostratigraphy, coeval strata are identified based on the geochemical patterns rather than facies and stratal relationships. As sequence stratigraphic analysis and chemostratigraphy are independent of each other, they can be complimentary tools for correlation, and must be consistent with each other. Thus the coeval surfaces identified via sequence stratigraphic analysis (e.g. parasequence boundaries) cannot cross a chemostratigraphic event, but could be contained within long lived chemostratigraphic event.

Some advantages that chemostratigraphy has over other stratigraphy methods is the ability to correlate with greater lateral continuity than with just facies. Lateral facies changes can complicate the correlation of strata; however correlation of similar isotopic signatures relies on excursion matching, and is independent of lateral facies changes. Chemostratigraphic correlations are limited by the density of sampling and quality of the data, but not by lateral facies variability. Further, chemostratigraphy can provide additional correlation events within the sequence stratigraphic framework where sequence or parasequence boundaries cannot be identified.

Geologic Background

The Blackhawk Formation and the Castlegate Sandstone were deposited in the Sevier

Foreland Basin along the western edge of the Cretaceous Western Interior Seaway (KWIS)

during the Late Cretaceous in the Campanian (Fig. 1). The sediment source for the Blackhawk

Formation and the Castlegate Sandstone was the Sevier Orogenic Belt, a fold and thrust belt

located west of the study area (Jordan, 1981). The paleolatitude of the study area during the

Campanian was 42°N (Kauffman, 1977). The paleoclimate was subtropical to warm temperate

with seasonality (Parker, 1976). The Blackhawk Formation and the Castlegate Sandstone are

exposed in the Book Cliffs from eastern Utah to western Colorado. The study area is Tuscher

Canyon, located approximately 15 km northeast of Green River, Utah (Fig. 1).

The Blackhawk Formation and the Castlegate Sandstone contain nonmarine and marine

facies that were part of a series of prograding clastic wedges that intertongues with the Mancos

Shale (Fig. 2) (Van Wagoner, 1995). The Desert Member is the youngest of six

lithostratigraphic members that comprise the Blackhawk Formation. These members consist of

prograding clastic shorefaces and deltaic sandstones that prograded into the foreland basin due to

tectonic loading during thrust events in the orogenic belt (Jordan, 1981). The Desert Member

contains a regionally extensive IVF which is the focus of this study. The Castlegate Sandstone

contains a regionally extensive IVF that erosionally overlies the Blackhawk Formation, and in

places, truncates the IVF within the underlying Desert Member (Van Wagoner, 1995).

The sequence stratigraphy of the Blackhawk Formation and the Castlegate Sandstone has

been studied extensively because of the high quality exposures that extend for kilometers. Van

Wagoner (1995) divided the Desert Member into a highstand and lowstand systems tract. The

IVF of the lowstand systems tract rests erosionally on the underlying highstand strata, and is

truncated by the IVF of the overlying Castlegate Sandstone. The depositional facies and sequence stratigraphic framework of these strata was established by Van Wagoner (1995) and provides the stratigraphic framework for this study. Hoffmeister (2011), in a subsequent study on the overlying Castlegate Sandstone, provided a more detailed cross section which is used in this study (Fig. 3).

The Desert Member includes several systems tracts including the Grassy Highstand (HST), the Desert Lowstand (LST), the Desert Transgressive (TST), and the Desert Highstand systems tracts (Fig. 4). The Grassy HST occurs in the lower part of the Desert Member, and is incised by the Desert Sequence Boundary. The Desert Sequence Boundary is the basal contact of the Desert Depositional Sequence and is also the upper contact of the Grassy Depositional Sequence. The Desert LST lies above the sequence boundary and is comprised of the IVF investigated in the study area. The Desert LST is incised by the overlying Castlegate Sequence Boundary. In Tuscher Canyon, the Castlegate Sandstone consists entirely of the IVF of the Castlegate Depositional Sequence.

The Desert and Castlegate Sequence Boundaries separate strata into depositional sequences estimated to have a duration between 200,000 to 300,000 years (Van Wagoner, 1995). Based on ammonite stratigraphy of *Baculites asperiformis*, *Baculites maclearni*, and *Baculites obtusus* established by Fouch et al. (1983) and Obradovich (1993), Van Wagoner (1995) estimated the Castlegate Sequence Boundary at 79 Ma. This date was proposed using the Cretaceous Time Scale of Obradovich (1993). Using the revised time scale of Gradstein et al. (2012), the date of the Castlegate Sequence Boundary is now estimate at 80.5 Ma (Fig. 3). The new ammonite dates are 80.21 +0.57 Ma for *Baculites asperiformis*, 80.67 +0.46 Ma for *Baculites maclearni*, and 80.97 +0.30 Ma for *Baculites obtusus*.

6

Global $\delta^{13}C$ marine chemostratigraphic curves have been generated for the Middle to Late Cretaceous with several large scale correlative events (Jarvis et al., 2006; Jenkyns et al., 1994). Several Middle to Late Cretaceous events have been identified including the Albian/Cenomanian Boundary Event, the Mid-Cenomanian Event, the Cenomanian/Turonian Boundary Event, the Late Turonian Events, the Santonian/Campanian Boundary Event, the Mid-Campanian Event, and the Late Campanian Event (Jarvis et al., 2006). The Jarvis et al. (2006) curves are utilized in this study.

METHODS

A $\delta^{13}C$ chemostratigraphic analysis and a sequence stratigraphic analysis of several well preserved paleosols and the associated non-marine strata within the IVF were conducted in this study. Field work was conducted in Tuscher Canyon, in the southern Book Cliffs, near the town of Green River, Utah. The sampling interval began in the lower shoreface in the Grassy HST of the Desert Member. Sampling progressed up-section, across the Desert Sequence Boundary into the IVF of the Desert Member, and across the Castlegate Sequence Boundary into the IVF of the Castlegate Sandstone. The IVF of the Desert Member contained several facies: inclined heterolithic strata of channel-fill sandstones, to thinly bedded channel-fill sandstones and siltstones to overbank siltstones and paleosols. Samples were processed and analyzed for Total Organic Carbon (TOC) and $\delta^{13}C$ of organic carbon for chemostratigraphy.

Field Methods

Four sections were selected and measured (Tuscher 1, 2, 3, and 4) within Tuscher Canyon, Utah at 39°05'52.5"N, 110°02'218"W (Fig. 1). Sections were selected for lateral facies variability and for known locations of paleosols. Measurements and descriptions were taken at the decimeter scale using a Jacob staff, grainsize chart, and Munsell color chart. Tuscher 1

7

section is a composite section while Tuscher 2, 3, and 4 are single transects. The measured sections were corrected using LIDAR imaging and a previous correlation (Scheppy, 2000) to form a composite section. LIDAR images were taken and processed by Myer (2012).

Facies descriptions (Table 1 and Fig. 8) by Van Wagoner (1995), Scheppy (2000), and Hoffmeister (2011) were duplicated in this study to provide detail and to provide a framework for sample collection. Facies descriptions for the non-paleosol facies included the following: color, grain size, sedimentary structures, trace fossils, bedding surfaces, contacts, local lateral continuity and geometries of bedding. Trace fossils were identified using the Treatise of Invertebrate Paleontology (Häntzschel, 1962). Descriptions for the paleosols consisted of the following: color from fresh surfaces using Munsell Soil Color Charts, pedogenic structures, trace fossils, soil horizons, horizon contacts, and local lateral continuity and geometries. The paleosol facies were based on descriptions of hand samples and outcrop expression.

A total of 345 samples were collected through the sections for isotopic analysis. Hand samples of sandstone, siltstone and mudstone ranging on average from 10 to 15 cm in size were collected, as well as samples of a few milligrams of organic material, where available. Sampling was done regardless of facies and taken systematically at half meter scale intervals. To ensure the best results, additional samples were collected at decimeter scale intervals on the facies adjacent to sequence boundaries, within paleosols, along the top of channel-fill sandstones, within over bank deposits, and at locations of concentrated organic material.

Chemostratigraphic Analysis

Isotopic analysis was carried out at the University of Kansas Keck Paleoenvironmental and Environmental Stable Isotope Laboratory. Hand samples were drilled using 1 mm carbide bits to obtain approximately 1 gram of powdered sample. The organic material was pulverized

in a mortar and pestle. Samples for TOC and $\delta^{13}C_{org}$ were decarbonated using a procedure

modified after that of Midwood and Boutton (1998). Samples were combusted at 1060°C using

a Costech Elemental Analyzer connected via a CONFLO III to the inlet of a ThermoFinnigan

MAT 253 isotope ratio mass spectrometer. Carbonate samples were reacted at 75°C with 100%

phosphoric acid in a ThermoFinnigan Kiel III single sample acid dosing system connected to a

dual-inlet ThermoFinnigan MAT 253 isotope ratio mass spectrometer. The results were

corrected for the weight of the samples and graphed using the δ notation relative to VPDB

(Vienna Pee Dee Belemnite) standard where $\delta^{13}C=[(^{13}C/^{12}C_{sample}/^{13}C/^{12}C_{VPDB})-1]*1000$ at one

part per thousand (‰). The percent of TOC was calculated after decarbonation of the samples.

RESULTS AND INTERPRETATIONS

Chemostratigraphic Results

$\delta^{13}C_{org}$ and TOC analyses were conducted on the samples collected from the IVF of the

Desert Member, as well as those collected from the Grassy HST of the Desert Member and the

Castlegate Sandstone (Fig.5 and 6). Through all of the facies including the marine lower

shoreface strata and the fluvial channel-fill strata, the $\delta^{13}C$ data was reliable. TOC data for the

lower shoreface strata is low around 1%, indicating there was little organic carbon for analysis,

but this did not affect the calculated $\delta^{13}C$ results.

Tuscher 1

The $\delta^{13}C$ and TOC profiles for Tuscher 1 start at 0.5 m and extend to 23.6 m (Fig. 5 and

6). The minimum value for $\delta^{13}C$ in Tuscher 1 is -28.00‰ at 21 m and the maximum value is -

24.84‰ at 12.5 m. The minimum TOC value is 0.027% at 15.1 m and the maximum value is

1.27% at 2.5 m.

In the $\delta^{13}C$ curve for Tuscher 1, there is an overall increasing negative trend with values

between -25.52‰ at 0.5 m to -27.75‰ at 23.4 m. The values between 0.5 m to 5 m vary little

around -25.50‰. After 0.5 m, the $\delta^{13}C$ values shift 0.5‰ negative and the curve changes to

small negative and positive peaks. At 9 m, the profile trends more negative, -27.30‰, and then

increases by 2.74‰ between 11 m to 12.5 m in a prominent excursion. After this peak, the

values decrease by 2.53‰ until 14.5 m and then flatten out at -27.00‰. Starting at 16 m, the

data becomes variable with numerous positive and negative peaks with a magnitude of 2 to

1.50‰. At 21.0 m, the profile sharply trends positive at -25.60‰ and remains level until 22.1 m.

The values then sharply decrease to -27.85‰ at 22.4 m.

The TOC profile for Tuscher 1 exhibits very little change and remains constant around a

mean value of 1%. There is a noticeable increase of 1% percent between 21.1 m and 22.3 m and

another increase between 1.5 m and 2.5 m.

Tuscher 2

The $\delta^{13}C$ and TOC profiles for Tuscher 2 start at 0.5 m and extend to 29.1 m (Fig. 5 and

6). The minimum value for $\delta^{13}C$ in Tuscher 2 is -29.07‰ at 6 m, and the maximum value is -

19.84‰ at 14.6 m. The minimum TOC value is 0.024% at 15.6 m and the maximum value is

61.09% at 13.1 m.

Tuscher 2 exhibits two overall trends: from 0.5 m to 13.1 m, the profile curves positive

from -28.70‰ to -19.84‰, and from 13.1 m to 29.1 m the profile gradually trends positive

increasing 2.93‰. Tuscher 2 starts with a broad negative peak, -25.73 to -28.62‰, up to 2 m

then the values trend positive to -25.53‰ between 2 to 4.7 m. The profile then drops 3.40‰ into

a negative peak, followed by more positives values to -25.53‰ between 6.5 to 8.5 m. There is a

sharp small negative peak to -28.18‰ which is then followed by a positive spike in values, -

25.36‰, at 9 m. The values then remain steady until 10.8 m with a small negative peak of -

27.07‰ at 10 m. At 10.8 m, there is another positive spike to -24.10‰ with steady values until 12.6 m, with a small -25.99‰ negative peak at 11.5 m. This is followed by a sharp positive peak, -21.96‰, at 13.1 m with a subsequent more gradual negative peak of -26.02‰ at 14.1 m. A sharp prominent -19.84‰ peak is seen at 14.6 m, followed by a sharp drop -7‰ at 15.1 m. The values then stay steady with a positive trend from -26.88‰ to -21.60‰ between 15.1 and 21.6 m, with a -26.99‰ peak at 17.6 m, a -26.01 peak at 20.1 m, and a -23.64‰ peak at 20.4 m. At 22.6 m, there is a negative 3‰ excursion in values followed by two small positive peaks, -24.52‰ at 22.8 m and -23.18‰ at 23.6 m. The subsequent values then stay steady around -25.00‰ to 29.1 m.

The TOC profile for Tuscher 2 between 0.5 m and 10.5 m averages around 1% with little change. Between 10.5 m and 13.6 m, the percent TOC varies greatly in a series of sharp peaks with a maximum value of 61.09% at 13.1 m and a minimum of 0.1% at 11.5 m. The profile from 14.1 to 18.9 m is steady around 1%. From 19.0 to 29.1 m, there is another series of sharp highly variable peaks of values with a maximum of 56.43% at 25.6 m and a minimum 0f 0.1% at 22.6 m.

Tuscher 3

The δ^{13}C and TOC profiles for Tuscher 3 start at 0.1 m and extend to 23.6 m (Fig. 5 and 6). The minimum value for δ^{13}C in Tuscher 3 is -28.98‰ at 22.4 m and the maximum value is -21.22‰ at 10.1 m. The minimum TOC value is 0.025% at 6.5 m and the maximum value is 61.68% at 22.1 m.

Overall, Tuscher 3's profile is steady averaging -25.00‰ then changes to -26.00‰ from 6.5 to 12.0 m. There is a small prominent negative peak at -25.93‰ at the base of the curve, followed by a flat trend at -24.80‰, followed by another negative peak of -26.91‰ at 2.5 m.

11

The values then remain level around -24.50‰ until 6.5 m where they shift to approximately -26.00‰ with small peaks with magnitudes of 1‰ continuing until 9.5 m. The profile then trends positive into a prominent peak with a 5.52‰ change at 10.1 m. This peak is followed by a sharp negative drop to -25.88‰ followed by a small positive peak, -24.06‰, at 10.5 m. The values then remain steady averaging -25.00‰ until 16.2 m, with a peak of -26.74‰ at 12.0 m. A sharp negative peak occurs at 16.2 m of -26.62‰, followed by another negative peak, -28.40‰, at 17.0 m. The next values are variable between -22.32‰ and -26.27‰ until 21.2 m with a positive peak of -22.32‰ at 20.5 m. The profile then trends negative and very variable with values between -23.42‰ and -28.98‰ for the rest of the transect.

The TOC profile for Tuscher 3 is quite variable and mostly consists of high magnitude spikes at 40 to 50%. There are three intervals of near 1% TOC values: 1.5 to 3 m, 9 to 10.4 m, and 10.9 to 12.4 m. The greatest variability in TOC starts from 16.2 m up to the top of the profile.

Tuscher 4

The δ^{13}C and TOC profiles for Tuscher 4 start at 3.5 m and extend to 16.7 m (Fig. 5 and 6). The minimum value for δ^{13}C in Tuscher 4 is -29.45‰ at 11.2 m and the maximum value is -21.58‰ at 6.3 m. The minimum TOC value is 0.042% at 14 m and the maximum value is 65.19% at 12.0 m.

Tuscher 4 begins with an overall positive trend from -26.33‰ to -21.58‰ up to 6.3 m and after exhibits a negative trend in values, -21.58‰ to -29.45‰, to 11.5 m, where the profile then remains steady around -26.00‰. The values start with a positive trend shifting 4.75‰ with positive and negative peaks to 6.5 m. A sharp negative excursion at 6.5 m of -26.14 ‰ and the values stay steady until 7.3 m. This is followed by a sharp positive shift to -23.93‰ at 7.5 m,

and then values fall to -25.57‰ by 9 m with a small positive peak of -23.86‰ at 8.3 m. There is a prominent sharp peak at 9.25 to -23.58‰ followed by a sharp negative fall to-28.99‰ at 9.5 m. This is followed by a negative peak at 11.2 m, -29.45‰, followed by a prominent positive rise to -23.59‰ at 11.8 m. The values then rise and fall in a series of negative and positive peaks with values between -23.59‰ to -27.18‰ until 13.3 m. The profile then falls -3.35‰ at 14 m and trends steady averaging -26.50‰ until 16.7 m, with a small positive peak of -25.03‰ at 16.1 m.

The TOC profile for Tuscher 4 is variable with a series of sharp high magnitude peaks from 3.5 to 6.5 m with a maximum value of 50.96% at 4.5 m. Between 6.5 and 7.1 m, the values remain steady averaging 1% and between 7.2 and 9.5 m, values are highly variable with sharp peaks and a maximum TOC of 42.30% at 8.5 m. The profile is stable between 9.5 and 11.5 m, which is followed by high magnitude spikes in TOC until 14.0 m with a maximum of 65.19% at 12.0 m. The rest of the TOC profile remains flat with an average value of 1% with a spike in TOC of 39.84% at 16.6 m.

Chemostratigraphic Events

The $\delta^{13}C$ and TOC were plotted against the measured sections (Fig. 7) and eight events were selected from chemostratigraphic profiles based on the magnitude of the excursions as well as the shape of the $\delta^{13}C$ curves. The events are labeled A to H on the stratigraphic cross section. These events occur within the Grassy HST and the Desert LST.

There are three events within the Grassy HST, labeled A, B, and C. Event A is characterized by a broad symmetrical negative peak with an average magnitude of 1‰ and a range of values between -26.50‰ and -28.50‰. Event B also has a broad negative peak but has a 2.90‰ change in values and a range of -25.50‰ to -29.00‰. Event C is characterized as a sharp positive jump of 2.58‰ $\delta^{13}C$ followed by a steady trend at approximately -25.50‰.

There are five events within the IVF of the Desert Member, labeled D?, E, F, G, and H. Event D? is characterized by a small sharp asymmetrical negative peak with a magnitude of 2‰ and between -23.60 to -25.99‰. Event D? is labeled with a question mark because this event is less tenable than the other chemostratigraphic events. Event E is also asymmetrical but has a large positive excursion with an average magnitude of 5‰ with a range between -26.70‰ to -19.90‰. Event F is distinguished by a gentle asymmetrical negative peak with a magnitude of 1.40‰ and $\delta^{13}C$ between -25.06 and -26.70‰. Event G is asymmetrical starting at -25.50‰ and then gradually sifts positive 1.75‰, is followed by a sharper negative fall of 1.50‰. Event H is characterized by a large asymmetric negative excursion with a magnitude of 3.50‰.

Facies

Eight facies were defined based on sedimentary structures, trace fossils, grain size, bedding relationships, and vertical and lateral geometries in bedding. Facies 1 and 2 are within Grassy HST of the Desert Member and includes interbedded hummocky cross-stratification (HCS) and thinly bedded siltstone (facies 1), and amalgamated HCS sandstones (facies 2). Facies 3, 4, 5, 6, and 7 occur in the IVF of the LST in the Desert Member and include tidally influenced inclined heterolithic strata (facies 3), thinly bedded fluvial sandstones (facies 4), overbank siltstones (facies 5), and the paleosol facies (6a, 6b, and 7). Facies 8, straight fluvial sandstones, is within the Castlegate Sandstone. Facies 1 to 5 and 8 are summarized in Table 1 and Figure 8. The descriptions of these facies are consistent with the previous work on facies published by Hoffmeister (2011), Scheppy (2000), and Van Wagoner (1995).

Paleosol Descriptions

There are two types of paleosols present: Protosols (facies 6a and 6b) and paleo-Histosols (facies 7). The classification system proposed by Mack (1993) is used for paleosol classification.

Paleosols are classified based on hand samples and field descriptions. The Protosols have been subcategorized into paleo-Entisols (facies 6a) and paleo-Inceptisols (facies 6b) using the Retallack (1990) classification system. Horizons and pedogenic features were identified using US Soil Taxonomy (Soil Survey Staff, 2010) and Soils of the Past (Retallack, 1990).

Protosols are weakly developed paleosols that contain pedogeneic features, however, the features are not mature enough for further paleosol classification (Mack et al., 1993). Paleo-Entisols are considered the least developed paleosol and usually exhibit rooting with very poorly developed pedogenesis (Retallack, 1990). Paleo-Inceptisols have undergone greater pedogenesis and contain more pedogeneic features than Paleo-Entisols, however they still lack the developed horizons necessary for more mature soils (Retallack, 1990).

Paleo-Entisols are the most common paleosols seen within the area studied. In Tuscher 2, there is a paleo-Entisol 1.5 m thick at 21 m (Fig. 7). In Tuscher 3 there are two paleosols: a 50 cm thick paleo-Entisol at 16 m and a 1.5 m thick paleosol at 22 m (Fig. 9a and 9b respectively). In Tuscher 4, there is a 40 cm thick paleo-Entisol at 12 m. The paleo-Entisols lack epipedons and may contain weak A horizons. The A horizon is dark gray (2.5 Y 4/1) and contains platy peds with abundant rooting, clay lined tubules (Fig. 10c), and disseminated organic matter (Fig. 11c). Rhizoliths are either thin (1 to 2 mm) and slightly sinuous with lengths between 3 and 15 cm (Fig.10d) or uncommon thick (1 cm) rhizoliths 10 cm in length (Fig. 10b). The A horizon's upper surface is truncated by overlying fluvial channels and is sharp and uneven. The lower bounding surface is gradual and wavy. Underlying the A horizon is a C horizon that has different coloring and lithology depending on the parent material type. The paleo-Entisols that developed on overbank sediments are dark grey (N4/ I n N/gley) siltstone while the paleo-Entisols that overly channel-fill sandstones are light grey (5YR/7.1) (Fig. 10a and 10b

respectively). The C horizon is rooted with disseminated organic matter and compressed coalified tree limbs but retains relict bedding from the parent material (Fig. 11d). There are thin 1 to 2 mm rhizoliths 2 to 10 cm in length and uncommonly there are 1 cm thick and sinuous rhizoliths (Fig. 10a). The lower boundary is gradual to diffuse and wavy to irregular in shape.

There are two paleo-Inceptisols within the IVF of the Desert Member. Tuscher 2 has one paleo-Inceptisol with a thickness of 2 m at 27 m and Tuscher 4 has a 70 cm thick paleo-Inceptisol at 9 m (Fig. 12). These paleosols have ochric epipedons because the horizons lack enough organic material and dark coloring to be considered a more developed epipedon (Retallack, 1990). The ochric epipedon (upper horizon) is underlain by a cambic horizon, which is characterized by a lack of parent rock structure, some pedogeneic alternation, and higher chroma than the underlying horizons (Retallack, 1990). Weathered parent material underlies the cambic horizon. The A horizon is thin averaging 5 cm, is comprised of ochric siltstone with platy peds, and is heavily rooted. The rhizoliths are thin, 1 to 2 mm, and straight to sinuous with lengths between 3 to 10 cm in length. The overlying truncation surface is sharp and erosional. The underlying paleosol horizon boundary is clear and is smooth to wavy. The underlying cambic horizons consist of one or more Bw horizons followed by a C horizon. The Bw horizons are dark grey (7.5YR 4/1) siltstone with blocky angular peds (Fig. 11a), rooting, and disseminated organic matter. The rhizoliths are similar but less abundant compared to the A horizon. The boundary between the C and Bw horizons and those separating the Bw1 and Bw2 horizons are gradual to diffuse and are smooth to wavy in shape. The C horizon has relict bedding but is rooted to a lesser degree than the Bw horizons.

Paleo-Histosols are paleosols that contain coalified peat horizons indicating that they were waterlogged part of the year and contained high concentrations of organic matter (Mack et

al., 1993). There are three different paleo-Histosols within the IVF. Tuscher 2 has a 2.7 m paleo-Histosol at 19.5 m including a 30 cm coal horizon and a 1 m paleo-Histosol at 23 m including a 5 cm coal horizon. Tuscher 4 has a 1.5 m paleo-Histosol including a 17 cm thick coal horizon (Fig. 13). A previously reported paleo-Histosol within Tuscher 3 was not observed in this study, and is believed to be within the covered section near 13 m (Scheppy, 2000).

The paleo-Histosols contain a histic epipedon, which is characterized by a high organic matter fraction that is often waterlogged (Retallack, 1990). The histic epipedon is underlain by a cambic horizon followed by a weathered and occasionally rooted C horizon. The histic O horizon contains banded coal that is characterized as duroclarain coal, containing thin bright and dull coal layers with proportions of 40 to 60% each, using the Diessel (1992) classification. The O horizons in the paleo-Histosols are 5 to 30 cm thick and are black (10YR 2/1). It contains lenses of bright coal from compressed coalified tree limbs, unidentified plant leaf litter, and orange-red pebble to coarse sand-sized rounded amber. The upper horizon boundaries are sharp and distinct and locally scoured. The lower horizon boundaries with the A and cambic horizons are clear and smooth to wavy.

The O horizon is followed by either an A horizon or the underlying cambic horizons. The A horizon is dark grey (5Y 4/1) siltstone with medium platy peds and is on average 25 cm thick. The A horizon contains lenses of coal from compressed downed tree limbs and rounded amber. The A horizon contains persistent oblique vertical fractures that possibly could be evidence for rooting. The lower horizon boundary is gradual to diffuse and is wavy. The cambic horizons of the paleo-Histosols consist of a Bw horizon that gradually transition into a C horizon. The Bw horizons are gray (5Y 6/1) very fine lower sandstone and on average 10 to 30 cm thick. The Bw horizon lacks developed ped structure but has very little characteristics of the alluvial

parent material. The lower horizon boundary with the C horizon is diffuse.

Paleosol Interpretations

A paleosol's development (maturity) is the relative length of time for soil formation with all other soil forming factors (such as temperature, parent material, precipitation, and the degree of vegetation) remaining constant (Bown and Kraus, 1987; Retallack, 1988). Due to the degree of accumulated organic matter needed for coal formation, paleo-Histosols are considered to be moderately to strongly developed paleosols, depending on the coal thickness (Retallack, 1988). Woody coal seams with thicknesses between 2 to 20 cm are considered to be moderately developed paleosols. The paleo-Histosols in the IVF have an average 17 cm thick histic horizon which indicates they are moderately developed paleosols and with pedogenesis on average taking 10,000 years (Retallack, 1998). For paleosols that lack epipedon horizons, the degree of pedogenesis is used to estimate the degree of development so paleo-Entisols are considered to be very weakly developed and paleo-Inceptisols are considered to be weakly developed. The paleo-Entisols within the valley fill are very weakly developed and have an average pedogenesis period of 100 years (Retallack, 1998). The paleo-Inceptisols in the IVF are weakly developed with pedogenesis taking an average 1,000 years (Retallack, 1998).

The paleo-Histosols are laterally persistent throughout Tuscher Canyon where they have not been incised by overlying fluvial channels. The Protosols are also laterally persistent and have been truncated by overlying fluvial sandstones. The majority of the paleosols are truncated by fluvial erosion, are weakly developed, and are separated by fluvial channel-sandstones indicating that they are compound truncated paleosols as defined by Kraus (1999) and Wright and Marriott (1993). Compound paleosols are paleosols within a succession that have been separated by periods of sedimentation that are minimally weathered (Kraus, 1999). For

compound truncated paleosols to form, sedimentation rates had to have been unsteady and greater than the rate of pedogenesis (Kraus, 1999). The paleo-Histosols are overlain by a Protosol indicating they are compound paleosols which are similar to the compound truncated paleosols but lack the erosional surface from fluvial channel.

The paleosols are concentrated in the upper half of the IVF above facies 3 (Fig. 7). The change in the amount of paleosols is due to a shift in fluvial expression between the tidally influenced inclined heterolithic strata (facies 3) and the smaller, isolated, thinly-bedded fluvial sandstone (facies 4). The tidally influenced channel-fill sandstones have greater aerial extent causing greater deposition onto the flood plain. As Bown and Kraus (1987) concluded, pedogenesis is halted when burial occurs while erosion does not necessarily stop pedogenesis. With greater sediment input onto the overbank and floodplain, fewer soils formed in the lower half of the IVF. Since the fluvial units in the upper half are smaller with less truncation, the paleosols in the upper half had greater preservation potential.

In aggrading fluvial systems, the least developed paleosols were adjacent to the fluvial channel on the levees while the most mature soils developed on the floodplain (Bown and Kraus, 1987). The more mature paleosols were able to develop on the floodplain because they were farther from the active fluvial channel (Bown and Kraus, 1987). With greater distance from the channel, the sedimentation accumulation rate decreases and the duration of development between episodes of sediment increases (Bown and Kraus, 1987; Bridge and Leeder, 1979). Due to the very weak to weakly developed nature of the Protosols and their parent material, the paleo-Entisols and paleo-Inceptisols most likely developed on the levees of the fluvial channels. The Paleo-Histosols in turn developed on the floodplain adjacent to the fluvial channels.

Sequence Stratigraphy

In her regional work on the Desert Member, Hoffmeister (2011) divided the Desert IVF into three parasequences. Additional parasequences are identified in this study based on the paleosol and IVF facies. The tops of the paleosols were selected as parasequence boundaries due to their lateral continuity and their representation as a persistent subaerial exposure surface (Kraus, 1999). Two different types of paleosols can occur laterally at the tops of the parasequences due to the lateral variability in topography and location with respect to the active fluvial channel during deposition (Bown and Kraus, 1987). The shift from one paleosol type to another can be seen in parasequence 3, where a paleo-Inceptisol (Tuscher 4) is adjacent to a paleo-Entisol (Tuscher 3). In addition, parasequence boundaries were placed at the top of the channel fills. The datum for the stratigraphic cross section is a fixed datum (a coal) and was chosen for its lateral continuity (Scheppy, 2000). The parasequence boundaries were placed to be congruous with the chemostratigraphic events. Five parasequence boundaries within the IVF of the Desert Member were selected based on these criteria.

The sequence boundaries and systems tracts were not changed from the previous regional work of Van Wagoner (1995) and Hoffmeister (2011). The Desert and Castlegate sequence boundaries are laterally persistent and exhibit meters of relief through Tuscher Canyon. The channel scour coincident with both sequence boundaries contain a lag of plant debris, wood impressions, and rip-up clasts. The IVF of the Desert Member was deposited in the late LST to TST based on stratal attributes and the sedimentologic response to base level rise (Van Wagoner, 1995; Van Wagoner et al., 1990). Two parasequence boundaries are interpreted in Tuscher 1 and 2 within the Grassy HST in the Desert Member. These parasequence boundaries were placed based on the transition from facies 2 to facies 1 which represents a deepening in depositional

environments. This interpretation is consistent with that of Van Wagoner (1995).

DISCUSSION

The Desert IVF was part of the late LST to TST and contains aggradationally stacked to isolated fluvial channel-fill sandstones. According to Cleveland et al. (2007), immature paleosols with sandy alluvial parent materials indicate high depositional rates and an increase of accommodation. The rises in base level were discrete enough for the fluvial channels to avulse. The rise of base level was also episodic since the fluvial channels are not always vertically stacked or nested. Instead, the episodic changes in base level allowed the channels to meander through the incised valley, and to be separated by overbank siltstones.

The causes for base level rise cannot be determined. Base level rise in fluvial systems could be caused by eustasy, tectonic events, or paleoclimate. Some sequence stratigraphic studies on fluvial strata discount eustasy as a significant factor in base level change if fluvial systems are located far from the coast (Cleveland et al., 2007). The inclined heterolithic fluvial strata and other tidal signatures indicates that the IVF was close enough to the KWIS to have tidal influence (Shanley et al., 1992). Because of this, eustasy cannot be discounted as a factor that influenced base level.

Stages of Valley Fill

The IVF was separated into nine stages based on the interpreted detailed sequence stratigraphic framework of the IVF (Fig. 14). The term "stage" is used to refer to a single event or group of related events that contribute to the development of the incised valley. Using the pedofacies concept devised by Kraus (1987), a stage of fill within the IVF can be initiated from channel avulsion from a change in base level, which caused truncation of the underlying strata followed by subsequent infill of fluvial sediment. As the channel filled and migrated, overbank

21

sediment was deposited and pedogenesis began. Pedogenesis then ended with the start of the new stage that was initiated from aggradation in the IVF from a change in base level (Wright and Marriott, 1993).

Illustration of the stages can be seen in Figure 14. Some of the parasequences and parasequence boundaries in this schematic are seen in Figure 7 and are noted when present. (1) Stage 1 includes the incision into the Grassy HST from a lowering of base level at the initiation of the Desert LST. (2) Stage 2 starts with the deposition of the straight system fluvial unit coincident with a base level rise. This fluvial unit was not sampled in this study because it occurs lateral to the location of the measured section (this stage is not shown on Figure 7). (3) In stage 3, a second base level rise occurs followed by development of a new channel system which truncates the underlying strata of stage 2. This is recorded in the stratigraphic record as inclined heterolithic strata (tidally influenced channel fills) and subsequent paleo-Histosol pedogenesis. Stage 3 contains chemostratigraphic event D? in Tuscher 2 and 3 and parasequence 1 on Figure 7. (4) Stage 4 is associated with an increase in the rate of accommodation and initiates with a parasequence boundary, deposition of a new channel, and the deposition of thinly bedded fluvial sandstones and paleo-Histosol pedogenesis. Chemostratigraphic events E and F are within Stage 4. Event E was not recorded in the overbank siltstones of Tuscher 2 (see cross section, Figure 7; this parasequence is shown as PS2 in Figure 7). (5) Stage 5 starts with a base level rise, the formation of another parasequence boundary, which is followed by the deposition of the overbank siltstones and crevasse splay siltstones and sandstones of the new parasequence. The deposits of this parasequence are then modified by paleo-Inceptisol pedogenesis. Within stage 5 is chemostratigraphic event G (missing from Tuscher 3 due to lack of sampling through the covered section; this parasequence corresponds to PS3 in Figure 7). (6) Stage 6 initiates with a

22

new base level rise, a new parasequence boundary, and as with the two previous stages, deposition from a new channel and overbank system. These deposits are subsequently modified by paleo-Histosol pedogenesis. Stage 6 contains chemostratigraphic event H within the fluvial channel deposits. This parasequence corresponds to PS4 in Figure 7. (7) Stage 7 is associated with another increase in base level followed by a parasequence boundary development, and the fluvial deposits of the new parasequence. Pedogenesis is not recorded in this stage. This parasequence corresponds to PS5 in Figure 7. (8) Stage 8 starts with a new base level rise, formation of a new parasequence boundary and the deposition of new overbank sediments and isolated channels, followed by pedogenesis (this parasequence corresponds to PS6 in Figure 7). (9) In stage 9, truncation occurs from the incision of the Castlegate Sequence Boundary.

A minimum-average-age of each pedogenic event was derived from the paleosol maturity (Retallack, 1984). This allowed minimum-average-age estimates to be made for various stages. Stages 3, 4, and 6 have a 10,000 year minimum-average-age estimates because of the occurrence of the paleo-Histosols that developed at the end of these stages. Stages 5 and 8 have a 1,000 year minimum-average-age estimate due to the paleo-Inceptisols that developed during these stages. A minimum-average-age estimate was not interpreted for stages 1, 2, 7, and 9 because they lack observed paleosols within the study area. Any paleosols that may have developed within these stages were eroded by the succeeding stages of incised valley fill. The minimum-average-age estimates within the IVF are used to estimate a minimum age of the IVF of approximately 32,000 years. This minimum estimate does not incorporate the time represented by erosion and the deposition of the fluvial channels. Deposition within the IVF was episodic, with various rates associated with pedogenesis (Bown and Kraus, 1987). Van Wagoner (1995) estimated that the duration of the Desert Sequence at 200,000 to 300,000 years. The Desert IVF

23

that underwent pedogenesis represents just a portion of this time frame. Further studies using this stage fill approach on a greater lateral scale will more accurately predict the minimum-average-age of the IVF.

Considerations for Constructing Parasequence Stratigraphy

The parasequence interpretations are constrained by the facies descriptions within the IVF, the $\delta^{13}C$ data, and the previously published sequence stratigraphic framework (Hoffmeister, 2011; Van Wagoner, 1995). When identifying parasequence boundaries within an IVF, several concepts must be considered. For sediment to be deposited and stored above the fluvial channel, there must be a rise in base level leading to an increase in accommodation (Wright and Marriott, 1993). This process allows for fluvial deposits to stack upon overbank siltstones. For the channel to avulse and for channel deposits to stack vertically, aggradation must occur which requires an increase in base level. When channel and overbank deposits stack vertically, a parasequence boundary should be placed at the top of the channel-fill deposits. Parasequence boundaries are easiest to pick when a rapid rise in base level results in rapid flooding, and forms an abrupt contact (i.e., a sharp surface) separating fluvial deposits. When the aggradation rates are slow enough to allow fluvial and floodplain deposits to accrete vertically, the placement of the parasequence boundaries becomes more complicated, as with parasequence boundary 4.

Correlating $\delta^{13}C$ chemostratigraphy and sequence stratigraphy can add additional challenges. Parasequence boundaries and the chemostratigraphic events represent units of time within the strata. Excursions in $\delta^{13}C$ can record events that occurred within a few years to 1,000s of years within terrestrial systems (Cerling and Quade, 1993). The length of time for a particular chemostratigraphic event cannot be determined without additional dating techniques. Even though the age of each chemostratigraphic event cannot be determined, the $\delta^{13}C$ events

24

within the IVF may have a shorter duration than the parasequence boundary. Parasequence boundaries and chemostratigraphic correlations should not intersect. If this happened, it would imply that the parasequence boundary had a shorter duration than the chemostratigraphic event. Therefore, chemostratigraphic event E does not intersect parasequence boundary 1 in Tuscher 2.

For the greatest resolution, sampling for chemostratigraphy should be done at the decimeter scale or less. Fluvial events within IVFs have the potential to occur rapidly and in isolated events, therefore a greater resolution of sampling increases the likelihood to capture these changes. Channel-fill and related overbank deposits should be sampled with closely space vertical sections for a more complete analysis of the stages of valley fill.

Evaluation of Chemostratigraphic Analysis

The comparison of the $\delta^{13}C_{org}$ and TOC stable-isotopic data demonstrates that the sampling in spite of the different facies regardless of organic matter content, all yielded sound data. The lower shoreface deposits were expected to have very little organic matter, but only 10 μg of organic carbon was needed for a precise analysis. The amount of material processed to obtain 10 μg of organic carbon differed depending on the lithology of the sample, however, there is no correlation between TOC values and $\delta^{13}C$ values and sample size. The TOC data does not reflect the magnitude or the shape of the $\delta^{13}C$ events, indicating the events are driven by factors other than amount of organic carbon or post depositional oxidation of the organic matter. This comparison shows the efficiency of the sample processing and that a large scale study evaluating the chemostratigraphic profiles of the highstand and the lowstand facies in the Blackhawk can be conducted.

Paleoclimate

Parker (1976) and Hampson et al. (2005) completed paleoclimate studies from coals and

fluvial strata within the highstand events in the Blackhawk Formation: the paleoclimate was interpreted as humid and subtropical. Globally, there was a transition of hot to cool greenhouse conditions with high sea levels and elevated CO_2 during the Campanian (Huber et al., 2002; Jarvis et al., 2002). The paleosols from this study indicates that the paleoclimate of the incised valley of the Desert Member was humid and temperate to subtropical. There are a lack of slickensides, carbonate nodules, and other arid type ped features associated with drier paleosols such as paleo-Aridisols (Mack et al., 1993). The paleo-Histosols indicate there were periods of waterlogged conditions suggesting that there was excess precipitation to evaporation allowing for mires to form (Lottes and Ziegler, 1994).

Davies et al. (2005) found that there were extensive raised mires in the highstand of the older members of the Blackhawk Formation and that there were similar paleoclimatic conditions to what Parker (1976) and Hampson et al. (2005) concluded. When the paleoclimate of the HST is compared to the paleoclimate of the IVF within the Desert Member, there is not enough evidence to suggest there was any change in the paleoclimate. The histic horizons in the IVF paleosols are not as extensive or as thick as those seen the Sunnyside Coal, as reported by Davies et al. (2005). However, the thickness of coal deposits is mostly a function of the period of accumulation of peat material rather than the degree of precipitation (Retallack, 1990). The duration of pedogenesis in the HST should be much greater than that of IVFs where there is much greater variability in sedimentation rates and facies. It is likely then that the differences between the paleo-Histosols formed in the HST versus the LST are due to length of pedogenesis rather than the change in precipitation.

Based on the lack of systematic stable-isotopic changes throughout profiles, the stages within the IVF were most influenced by changes in the regional paleoclimate patterns rather than

26

changes in the global paleoclimate. The chemostratigraphic profiles that correspond to the stage boundaries and the paleosols lack a specific pattern in their excursions indicating that the initiation of a new stage and pedogenesis were not all responding to the same conditions. The regional climate controlled pedogenesis.

Based on the magnitude of the δ^{13}C profiles compared with the global curve or Jarvis et al. (2006), the IVF should correlate between the Santonian/Campanian Boundary Event and the Mid-Campanian Event (Jarvis et al., 2006). However, the chemostratigraphic data generated in this study was taken over to short a section and at a resolution that was too low for an accurate correlation with the global curves or with the large scale events. Van Wagoner (1995) had estimated that the sequences within the IVFs of the Desert Member and Castlegate Sandstone were on the order of 200,000 to 300,000 years while major events on global curves are on the scale of 1 Ma (Jarvis et al., 2002). Furthermore, sampling strategy resulted in under sampling of channel fills and flood plain deposits resulting in incomplete chemostratigraphic profiles. Greater sampling that covers a longer timeframe is needed to accurately place the isotopic data within the larger framework. Based on Van Wagoner's (1995) sequence duration interpretations, several members of the Blackhawk Formation and the Castlegate Sandstone should be analyzed for comparison into the global δ^{13}C curves.

CONCLUSIONS

The detailed facies analysis of the IVF paleosols with the δ^{13}C chemostratigraphic analysis led to a refined parasequence-level sequence stratigraphic interpretation of the Desert IVF. Within the fill, three moderately developed paleo-Histosols, three weakly developed paleo-Inceptisols, and four very weakly developed paleo-Entisols were described. The paleo-Histosols developed on the flood plain while the paleo-Entisols and paleo-Inceptisols developed on the

levee sediments. Based on the paleosols, the paleoclimate was humid and temperate to subtropical.

A $\delta^{13}C$ and TOC chemostratigraphic architecture was developed for the Desert Member. Eight chemostratigraphic events were selected based on the excursions within the $\delta^{13}C$ profiles. The $\delta^{13}C_{org}$ analyses were reliable for all of the facies described in this study including the lower shoreface facies within the Grassy HST of the Desert Member.

Based from the new paleosol descriptions and chemostratigraphy, six parasequences were selected within the IVF of the Desert Member. Parasequence boundaries were placed at the top of paleosols and fluvial channels. The new parasequence boundaries provide better resolution to the sequence stratigraphic framework within the IVF.

The IVF was part of the late lowstand to early transgressive systems tracts based from stratal attributes and fluvial aggradation. The fill was divided into nine stages. A minimum-average-age was determined for stages 3, 4, 5, 6, and 8 based on paleosol maturity within each stage. Stages 3, 4, and 6 have minimum-average-ages of 10,000 because they contain paleo-Histosols. Stages 5 and 8 have minimum-average-ages of 1,000 years since they contain paleo-Inceptisols. A total minimum-average-age for pedogenesis within the IVF is 32,000 years. These results prove that chemostratigraphy can be used in conjunction with sequence stratigraphy within terrestrial systems to develop a parasequence level interpretation. Vertical sampling at the 10 cm resolution within the fluvial channels and their associated overbank deposits would have improved the interpretations.

Using a synthesis of chemostratigraphy, sequence stratigraphy, and detailed paleosol facies work can help refine the stages and depositional history of an IVF. Understanding the stages of IVFs at the parasequence level allow for better predictions of fluvial channel locations

and stratal relationships with the overbank deposits.
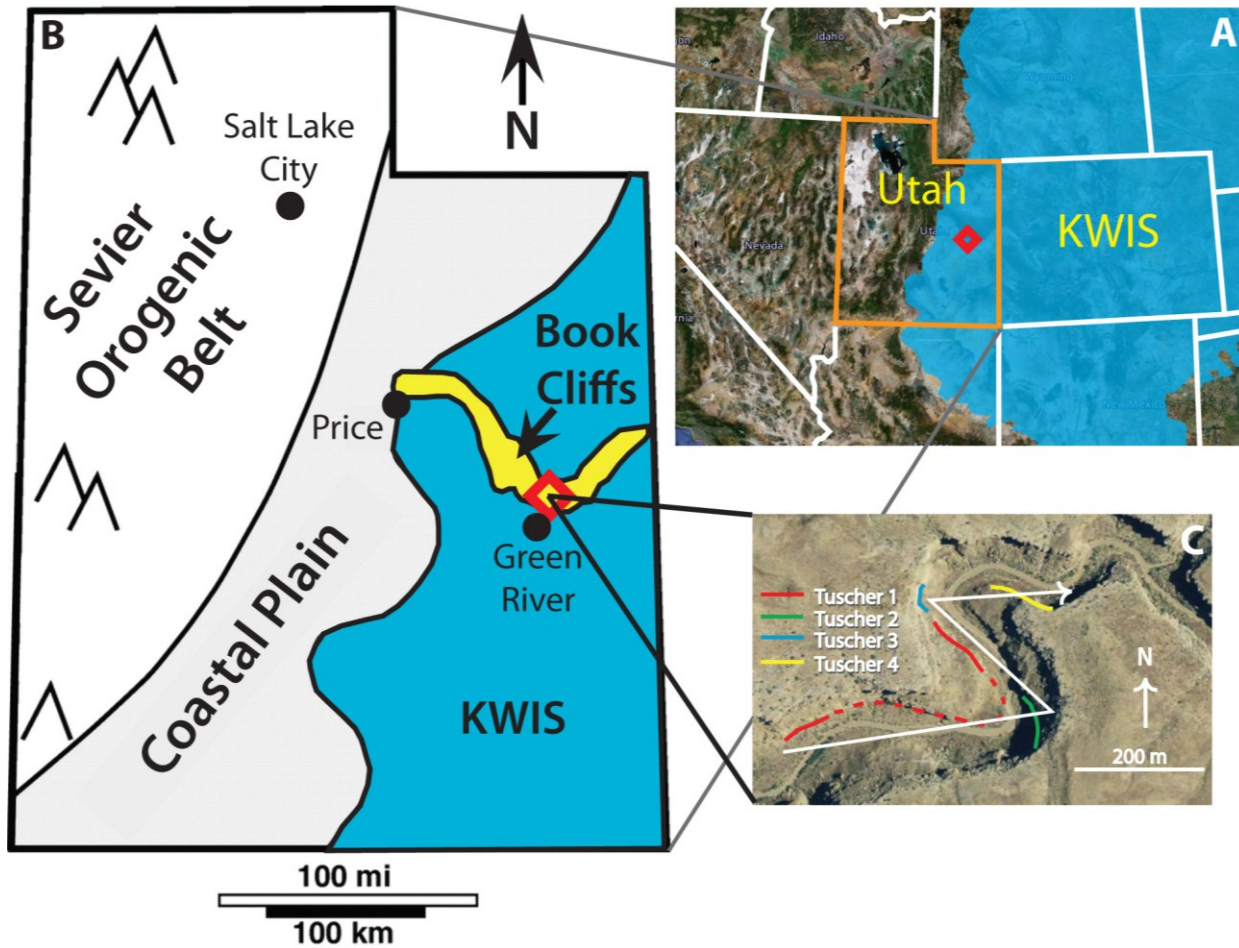
Figure 1. Map of the study location with respect to the paleogeography during the highstand deposition of the Blackhawk Formation and the present-day geography. (A) The Cretaceous Western Interior Seaway (KWIS) in blue with respect to Utah. (B) The paleogeography of Utah during highstand deposition depicting the KWIS and the Sevier orogenic belt with respect to the Book Cliffs. (C) Satellite image of Tuscher Canyon with the four transects in corresponding colors: Tuscher 1 is red, Tuscher 2 is green, Tuscher 3 is blue, and Tuscher 4 is yellow. The cross section line is in white. (Modified from Google Earth and (Houston et al., 2000)).
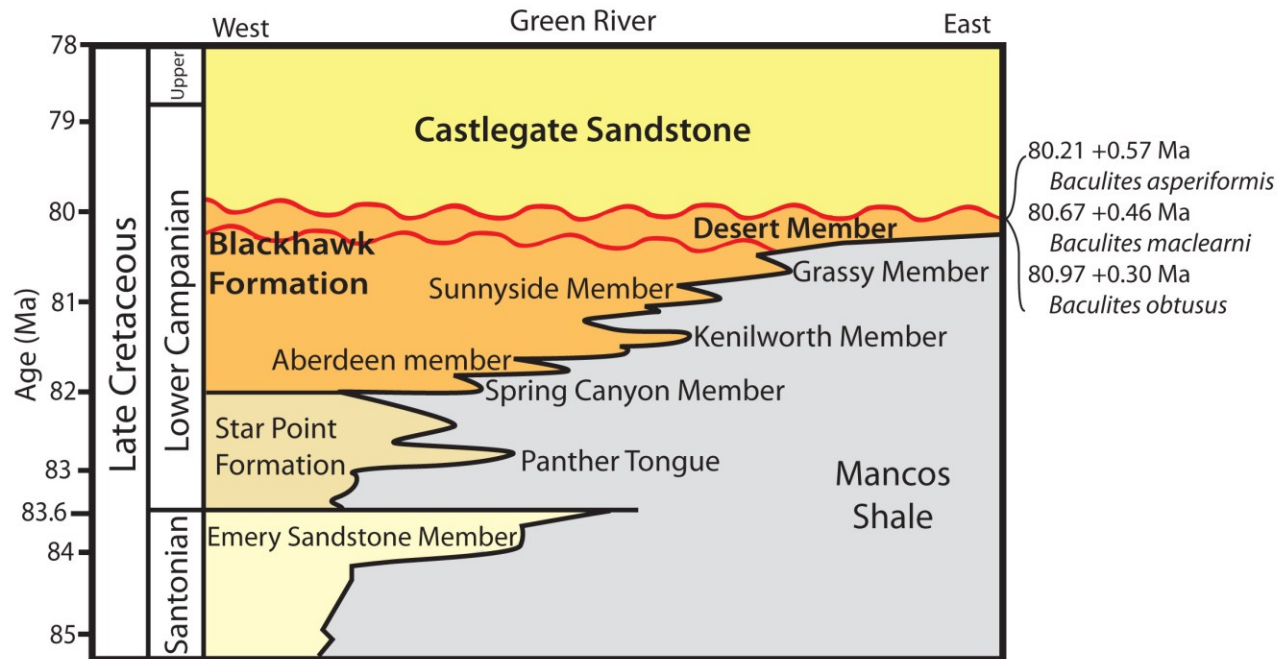
Figure 2. Lithostratigraphy of the Blackhawk Formation with the Castlegate Sandstone, Star Point Formation, and the Emery Sandstone. The erosional unconformity, red wavy line, separating the Blackhawk Formation and Castlegate Sandstone has been dated using ammonite biostratigraphy to 80.5 Ma (Fouch et al., 1983; Gradstein et al., 2012; Van Wagoner, 1995).
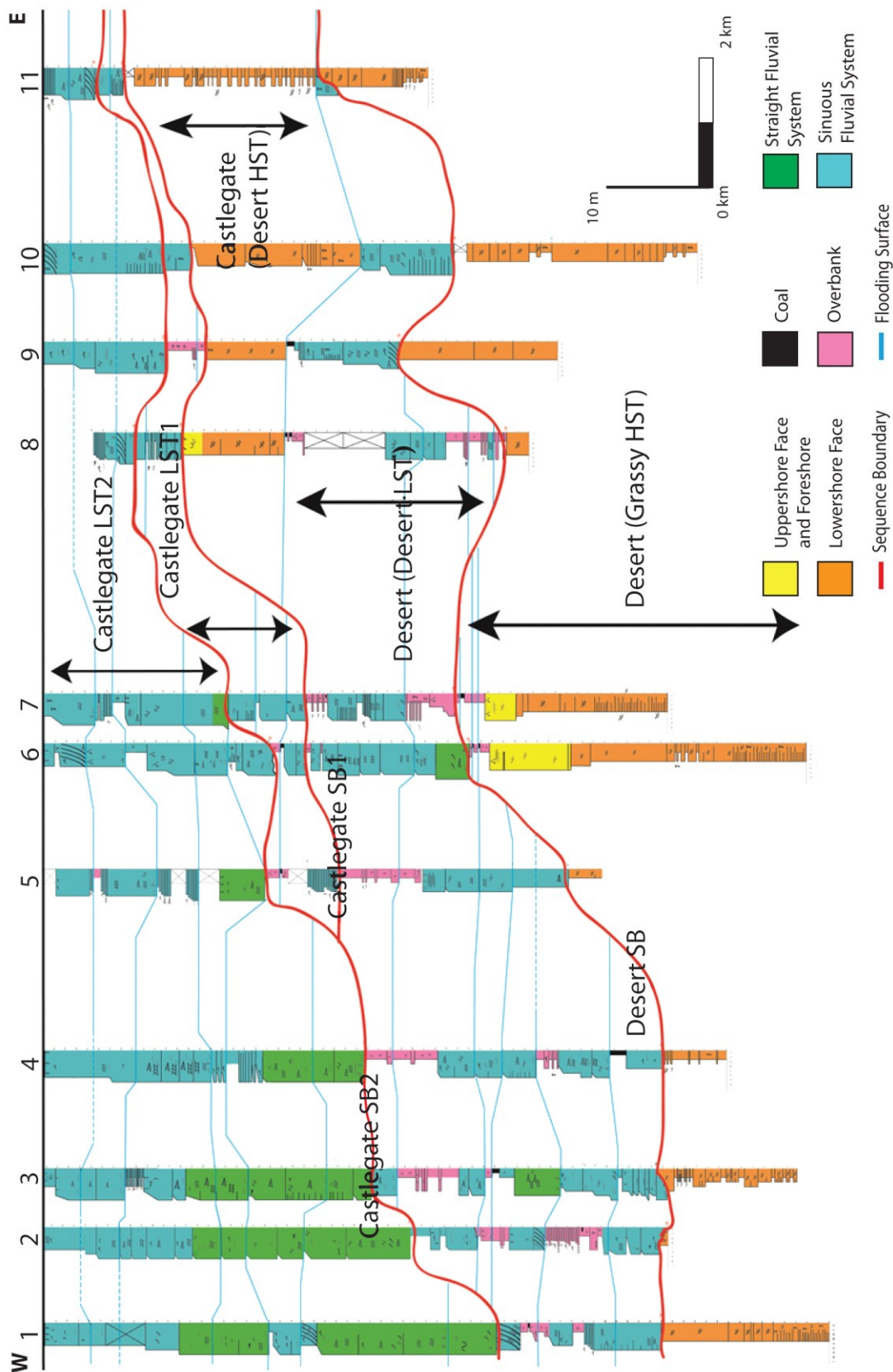
Figure 3. Detailed sequence stratigraphic framework of the Castlegate Sandstone and the Desert Member of the Blackhawk Formation proposed by Van Wagoner (1995) and modified by Hoffmeister (2011). Measured section 1 is located in Tuscher Canyon. (Modified from Hoffmeister (2011)).

Sequence Stratigraphic Nomenclature
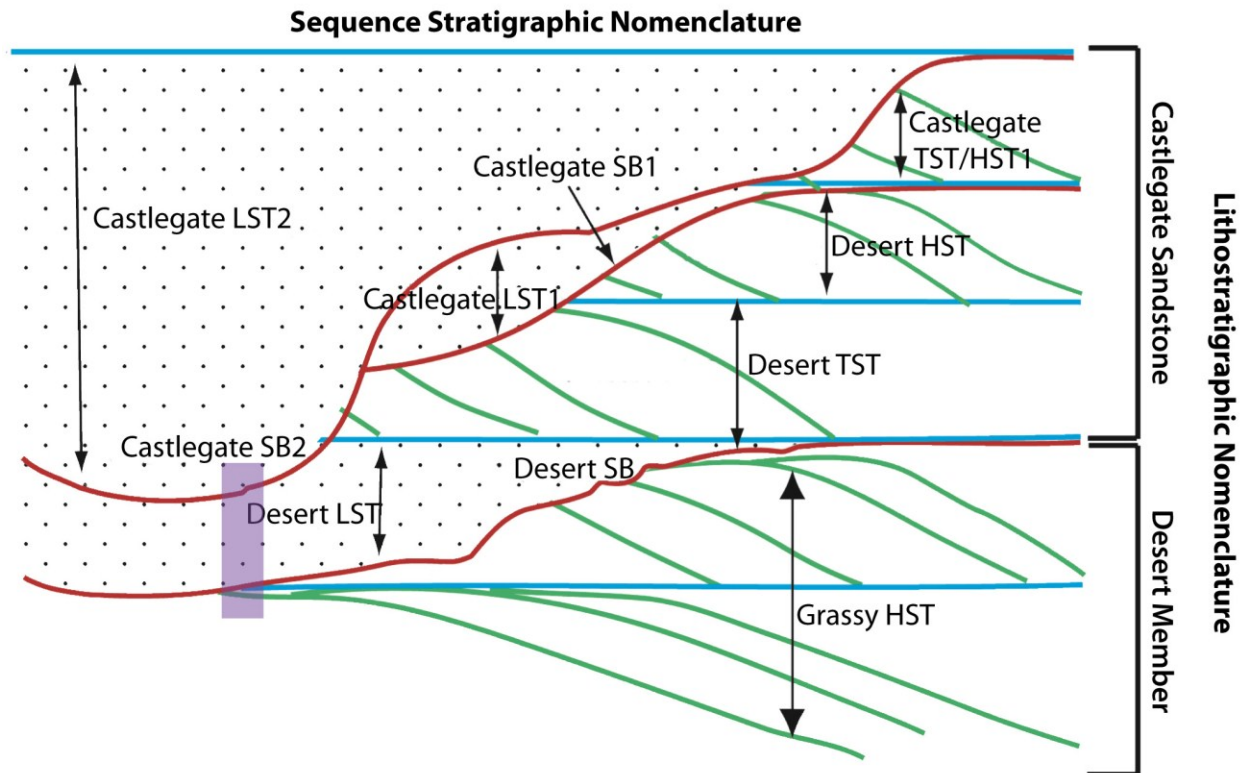
Figure 4. The lithostratigraphic and sequence stratigraphic nomenclature of the upper member of the Blackhawk Formation and the Lower Castlegate Sandstone, with terminology proposed by Van Wagoner (1995). The area studied in Tuscher Canyon is shaded in purple. (Modified from Hoffmeister (2011)).
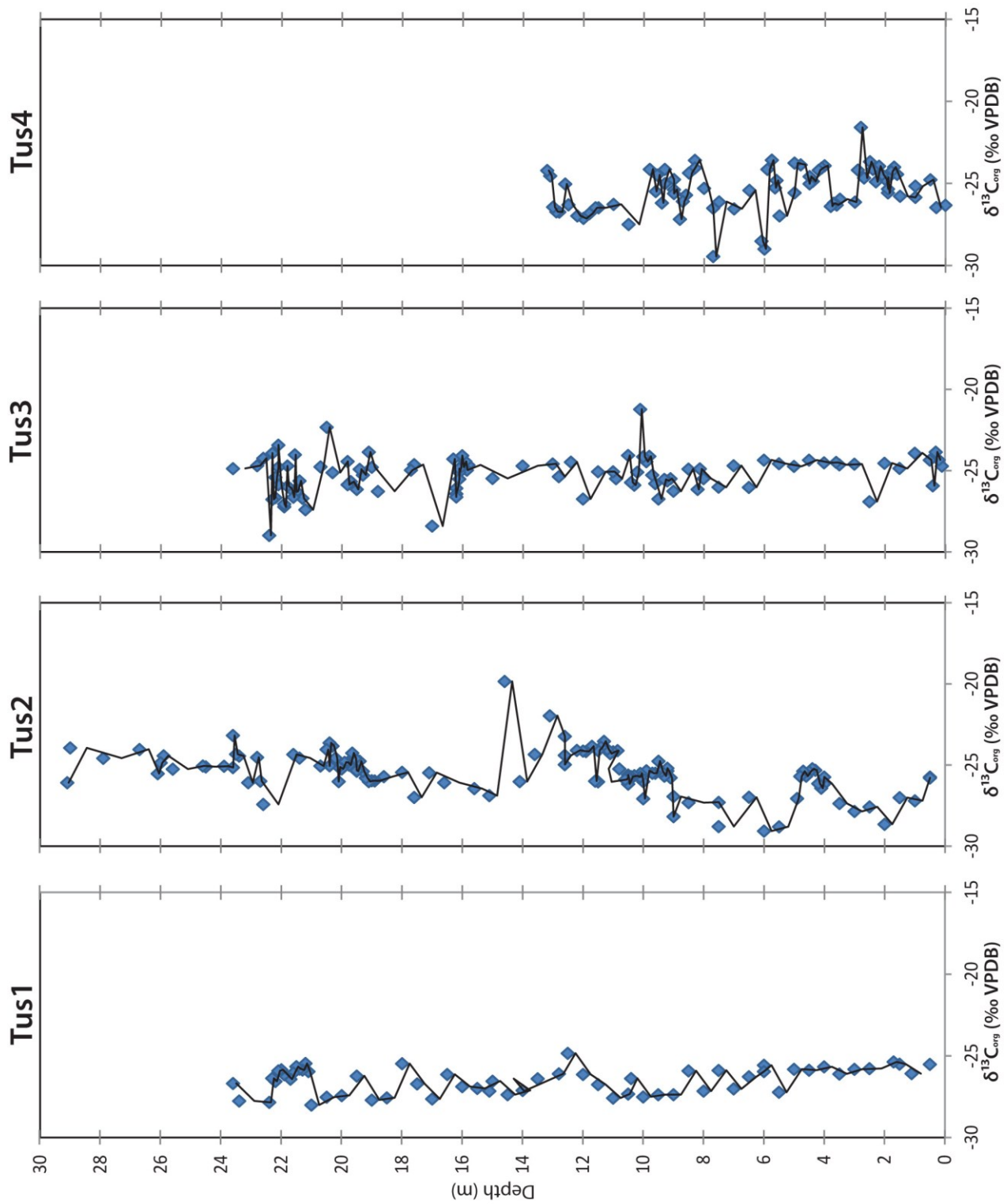
Figure 5. $\delta^{13}C$ stable isotope data with respect to depth for each transect.
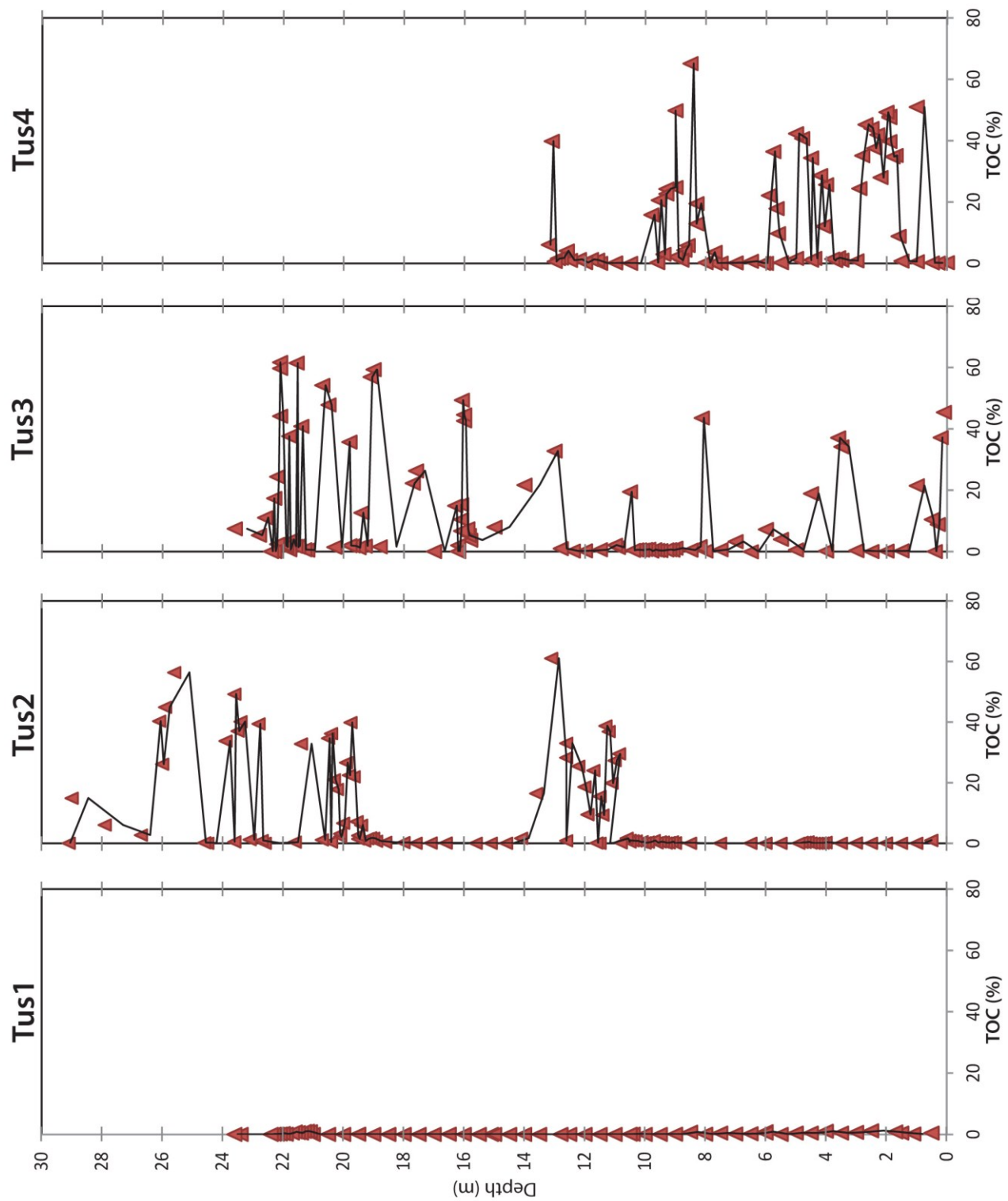
Figure 6. TOC stable isotopic data with respect to depth for each transect.
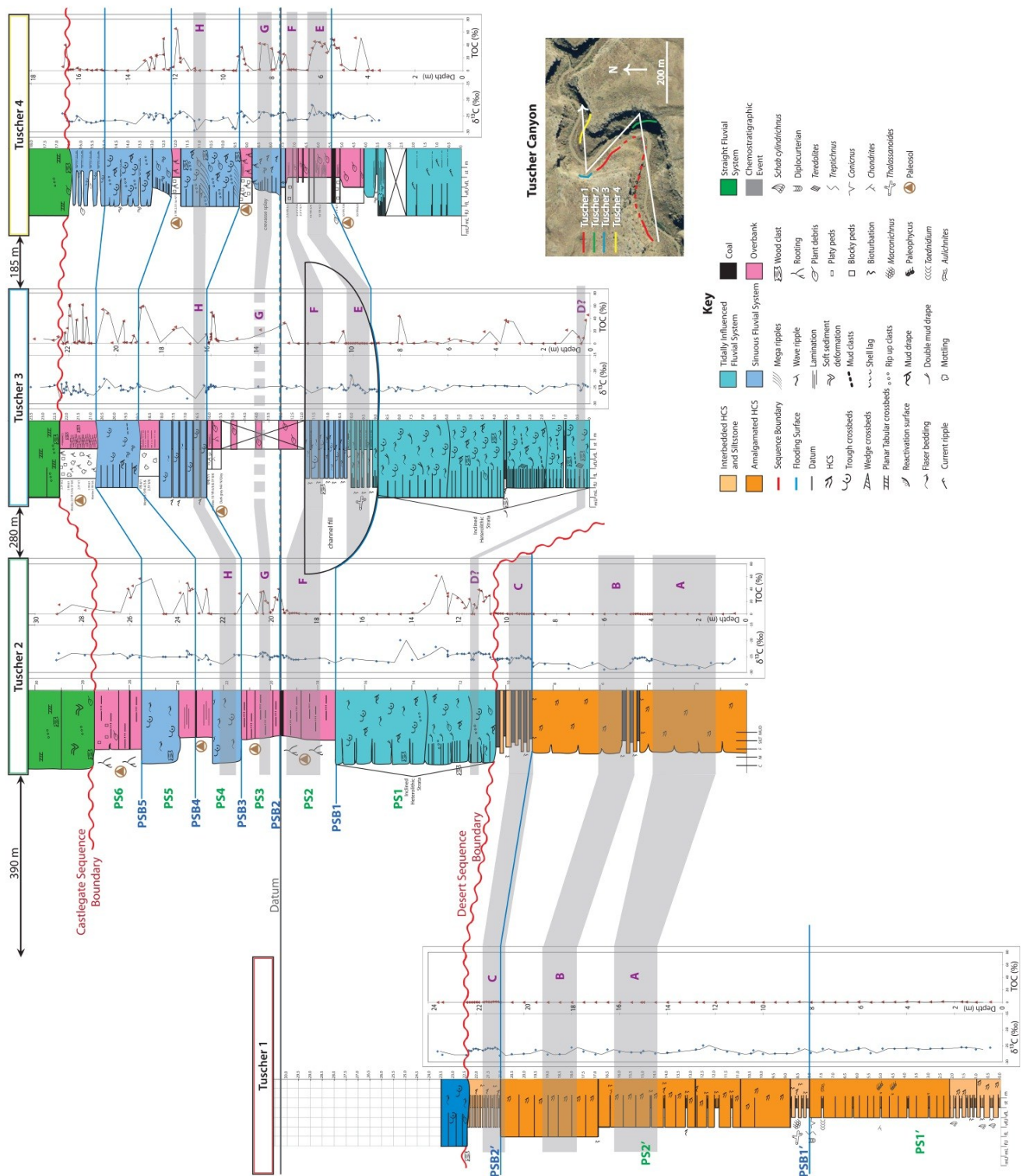
Figure7. Sequence stratigraphic cross section through Tuscher Canyon with $\delta^{13}C$ (blue graph) and TOC (red graph) for each measured section. The measured section locations within Tuscher Canyon are in the study area box. Tuscher 1 is a composite section. The gray shading is chemostratigraphic events labeled A through H. Parasequence boundaries are denoted PSB and parasequences PS.

Table 1. Facies descriptions from Tuscher Canyon, UT. Paleosol Facies (6a, 6b, and 7) are described in the results.

| Facies	Color and grain size	Sedimentary structures	Trace fossils and organic matter	Bedding	Geometry	Interpretation
8: Straight fluvial sandstones	Tan medium sublithic arenite	Large tabular to wedge cross bedding with reactivation surfaces, rip up clasts	*Teredolites*, wood debris, wood impressions	0.5m with local scouring	Base above sequence boundary contains lag of wood clasts and rip up clasts. Erosional channel base	Braided to straight fluvial channel sands
5: Overbank deposits	Medium to dark gray silt to brown gray mudstone	Massive to weakly laminated and bedded	Unidentified bioturbation, plant fragments, disseminated organic matter, amber, coal lenses	cm scale	Laterally continuous though scoured from channel sands	Overbank fines on coastal plain interfluve and paleosols
4: Thinly bedded fluvial sandstones	Light tan to gray lower fine sublithic arenite interbedded with gray heterolithic siltstone	Trough crossbedded, flaser bedding, soft sediment deformation, current ripples, wave ripples	*Thalassanoides*, unidentified horizontal bioturbation, plant debris, wood impressions, amber, disseminated organic matter	10 to 30cm thick sandstone interbedded with 0.5 to 3cm thick silt	Bedding is planar low angle lateral accretion. Erosional channel base	Meandering to straight fluvial unit bars
3: Tidally influenced inclined heterolithic strata	Light tan upper fine to lower medium sublithic arenite interbedded with black heterolithic organic silt	Heterolithic bedding, trough crossbeds with isolated sigmoidal bedding, current ripples, flaser bedding, organic mud drapes, double mud drapes, rip-up clasts	*Teredolites*, unidentified bioturbation, wood impressions, plant debris, disseminated organic matter, coarse sand to pebble size amber	10 to 30cm and bedsets 1m to 3m. Interbedded with heterolithic wavy 1 to .5cm organic silt in bedsets 10 to 20cm	Sandstone locally scoured, draped with organic silt. Beds and bedsets laterally accrete and pinch out. Heterolithic beds accrete vertically. Erosional channel base	Tidally influenced meandering unit bars of channel sands
2: Amalgamated HCS sandstones	Light tan very fine sublithic arenite with dark gray laminae	HCS with bioturbation into tops of bedding	Unidentified bioturbation	Average 0.5m	Amalgamated HCS, hummocks and swales scour contacts. Laterally scours into underlying beds; laterally continuous	Lower shoreface deposition, large stacked storm events. Proximal to facies 1
1: Interbedded HCS and thinly bedded siltstones	Light tan to light gray very fine sublithic arenite with dark gray laminae interbedded with medium gray siltstone	Siltstone is laminated, sandstone: HCS, wave ripples	*Paleophycus, Conicnus, Taednidium, Schab cylindrichnus, Treptichnus, Aulichnities, Diplocurterian, Macronichnus, Thalassanoides*, unidentified bioturbation	Silt 0.5 to 1 cm, sandstone average 10 to 30 cm	HCS: scoured contacts, pinches and swells laterally with thin organic lamina on bed surfaces. Unit is locally scoured	Background deposition of the lower shoreface with small storm events

37
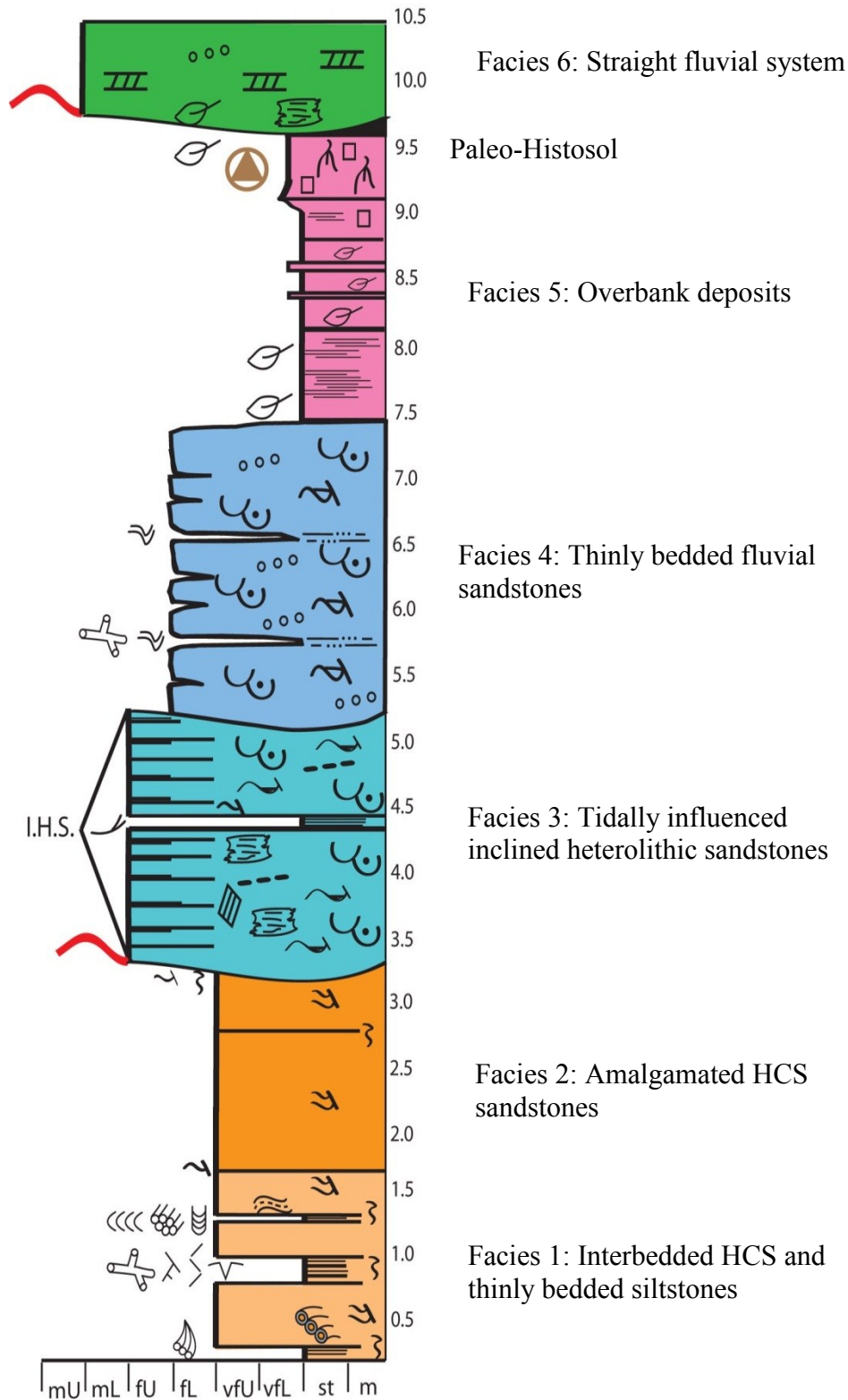
Figure 8. Idealized stratigraphic cross section of the facies described in Table 1. The red wavy line denotes the location of a sequence boundary and the symbol key is located in Figure 7.
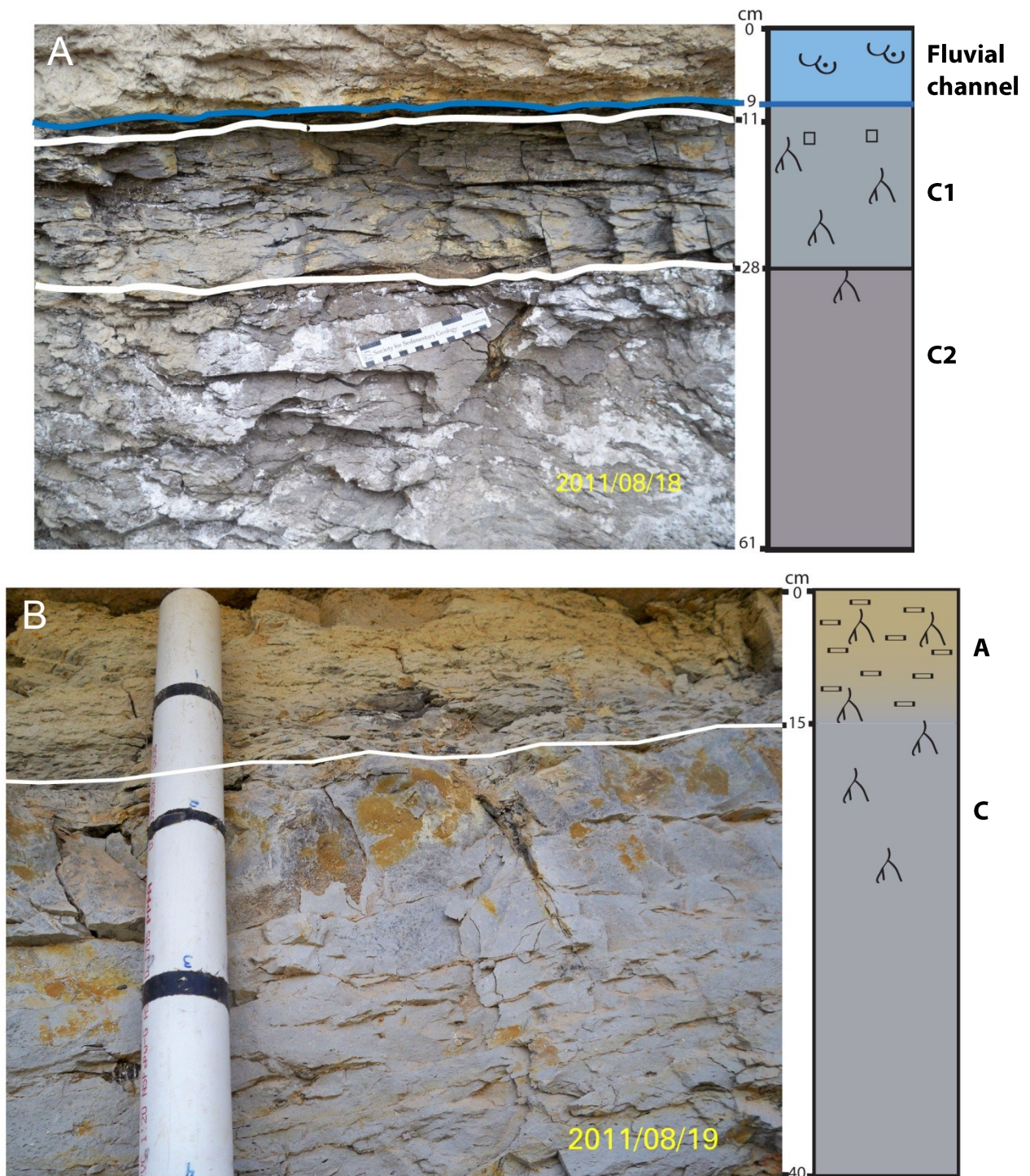
38

Figure 9. Paleo-Entisols (facies 6a) with interpreted horizons from Tuscher 3. (A) A paleo-Entisol that developed on overbank sediments that consists of two distinct rooted C horizons truncated by a fluvial channel. (B) Paleo-Entisol with a weak A horizon followed by a rooted C horizon that developed on fluvial channel sediments.
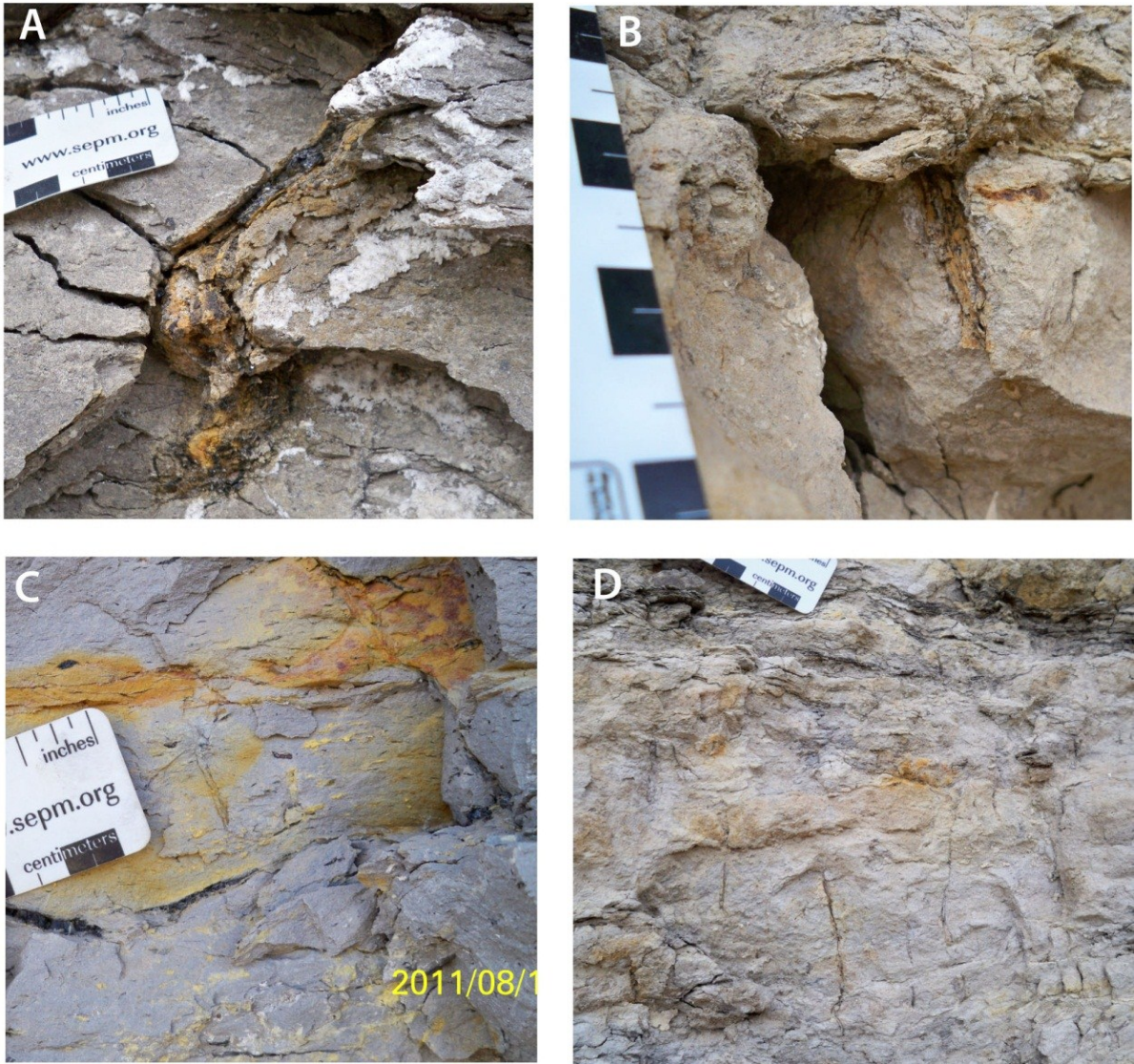
Figure 10. Root types seen in the Protosols of the IVF. (A) sinuous and thick (cm), (B) linear and thick, (C) clay lined tubules, and (D) thin (mm) slightly sinuous to straight roots.
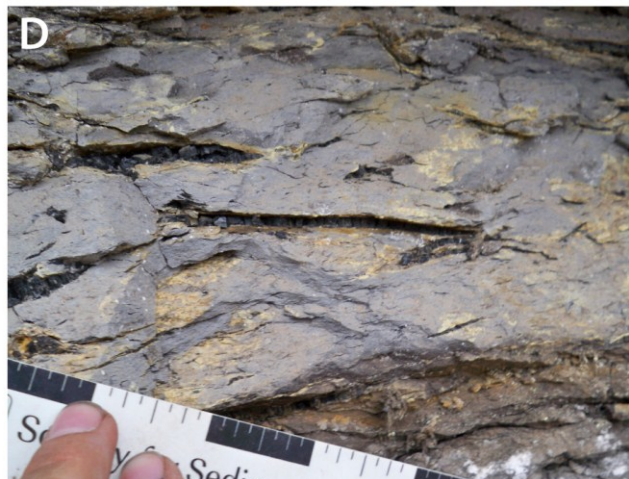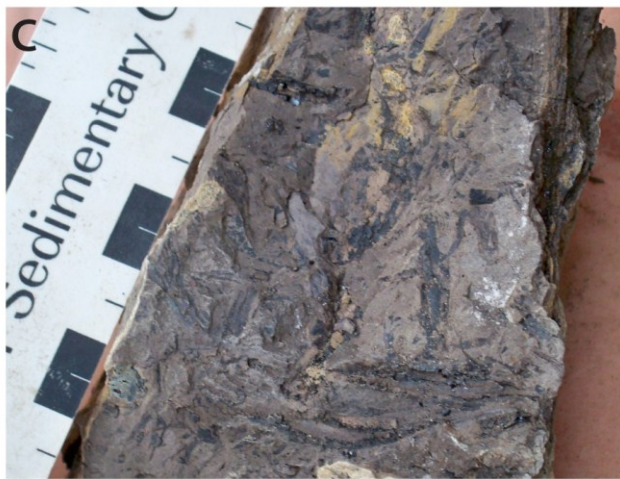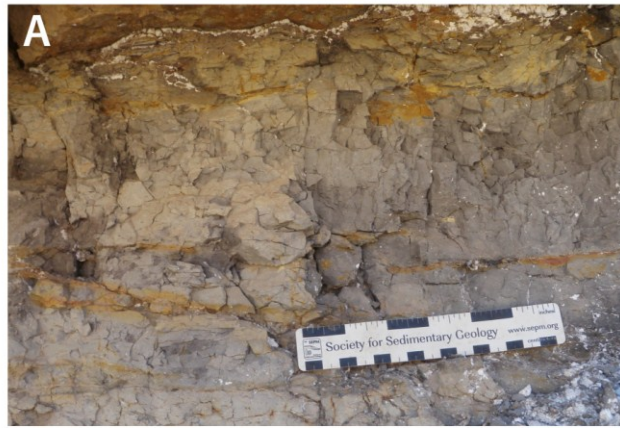
Figure 11. The pedogenic features seen within the paleosols of the IVF. (A) Blocky ped structure, cm scale, (B) rounded amber, usually a few mm in size, (C) disseminated organic matter (D) gleyed color (Dark gray N4/ N/Gley) and compressed coalified tree limbs.
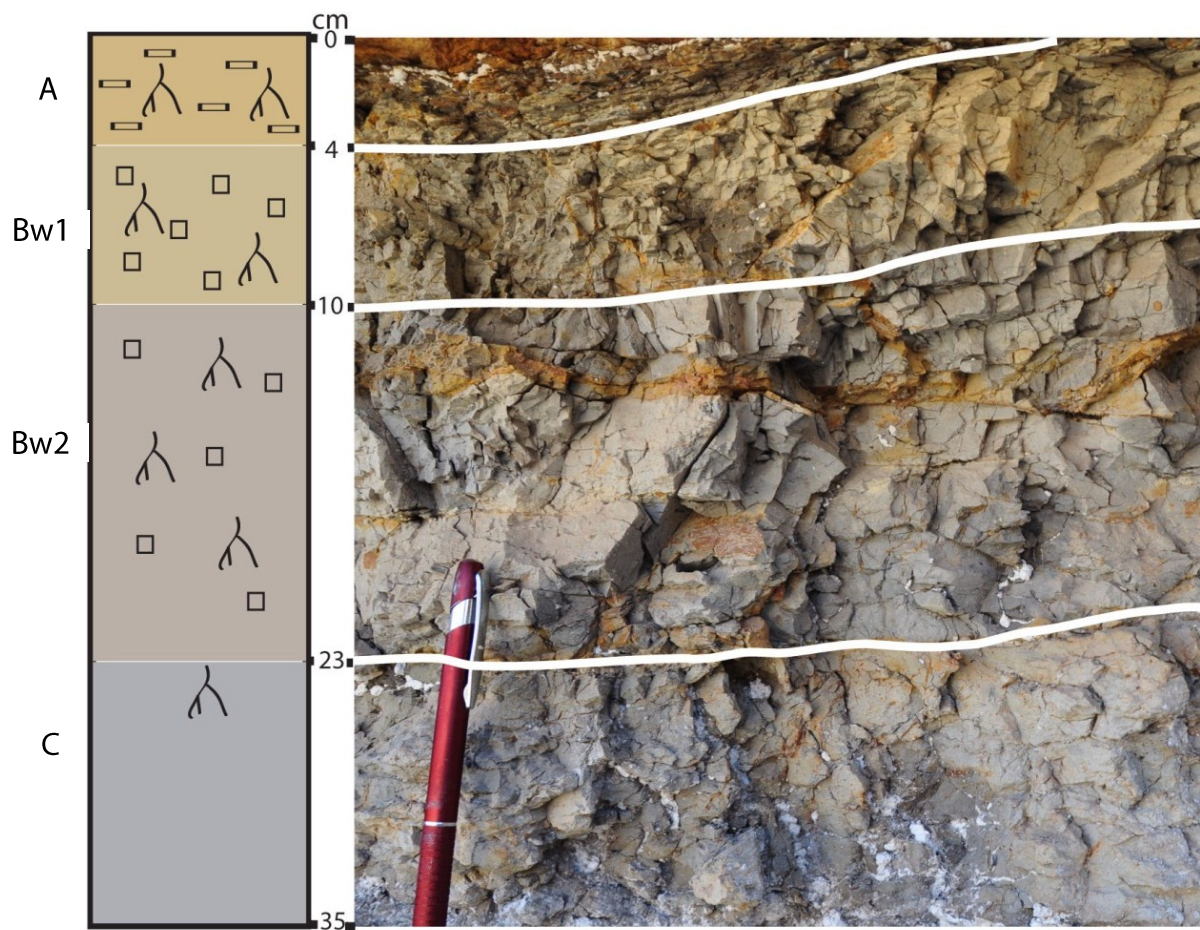
Figure 12. Paleo-Inceptisol (facies 6b) from Tuscher 4 with a pen for scale. This paleo-Inceptisol has a weak A horizon followed by two distinct rooted Bw horizons with angular ped structured and is underlain by a Cr horizon.
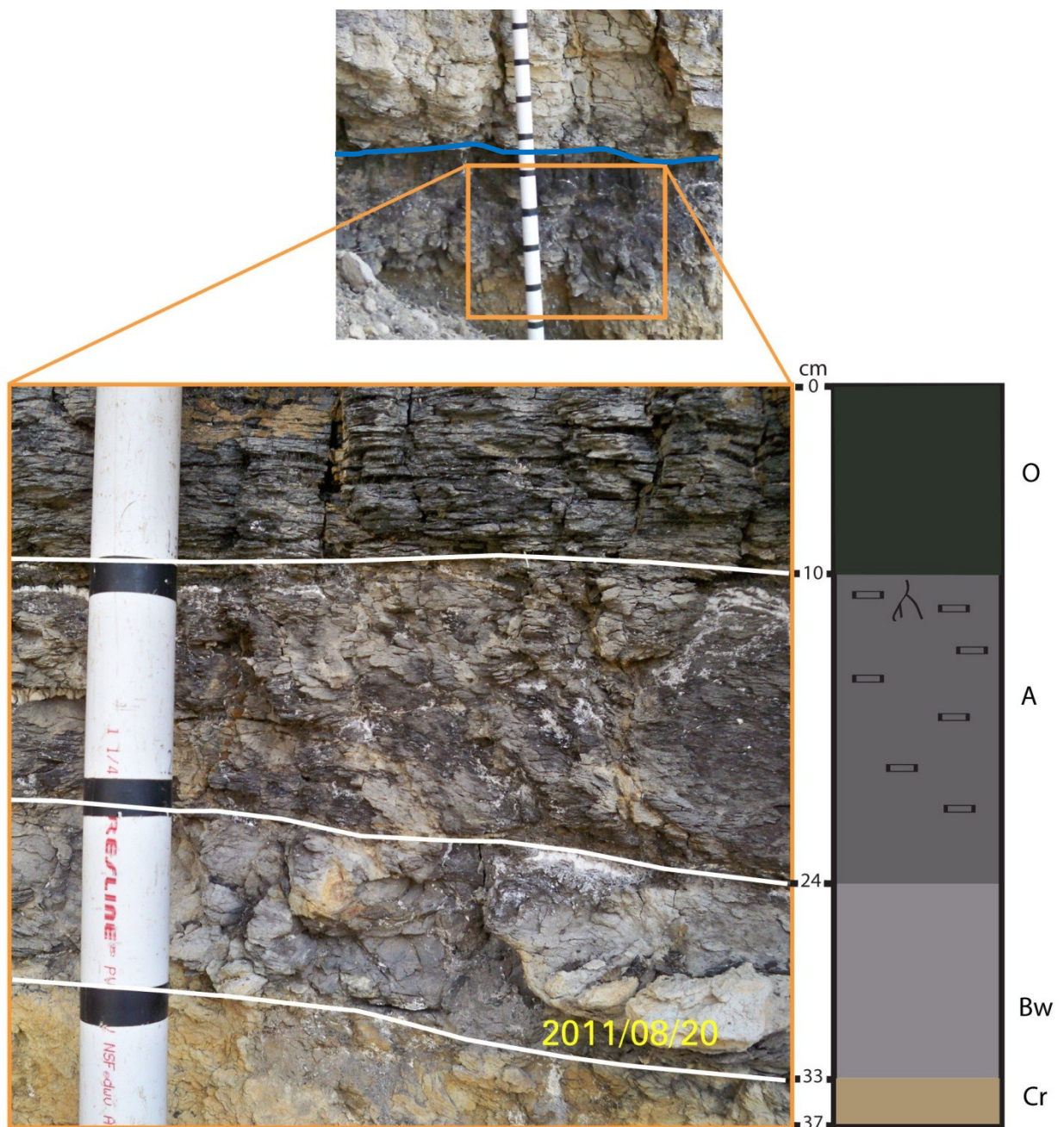
Figure 13. Paleo-Histosol (facies 7) from Tuscher 4. This paleosol has a coal O horizon that is followed by a platy A horizon and a weak Bw horizon that is underlain by a sandy Cr horizon.
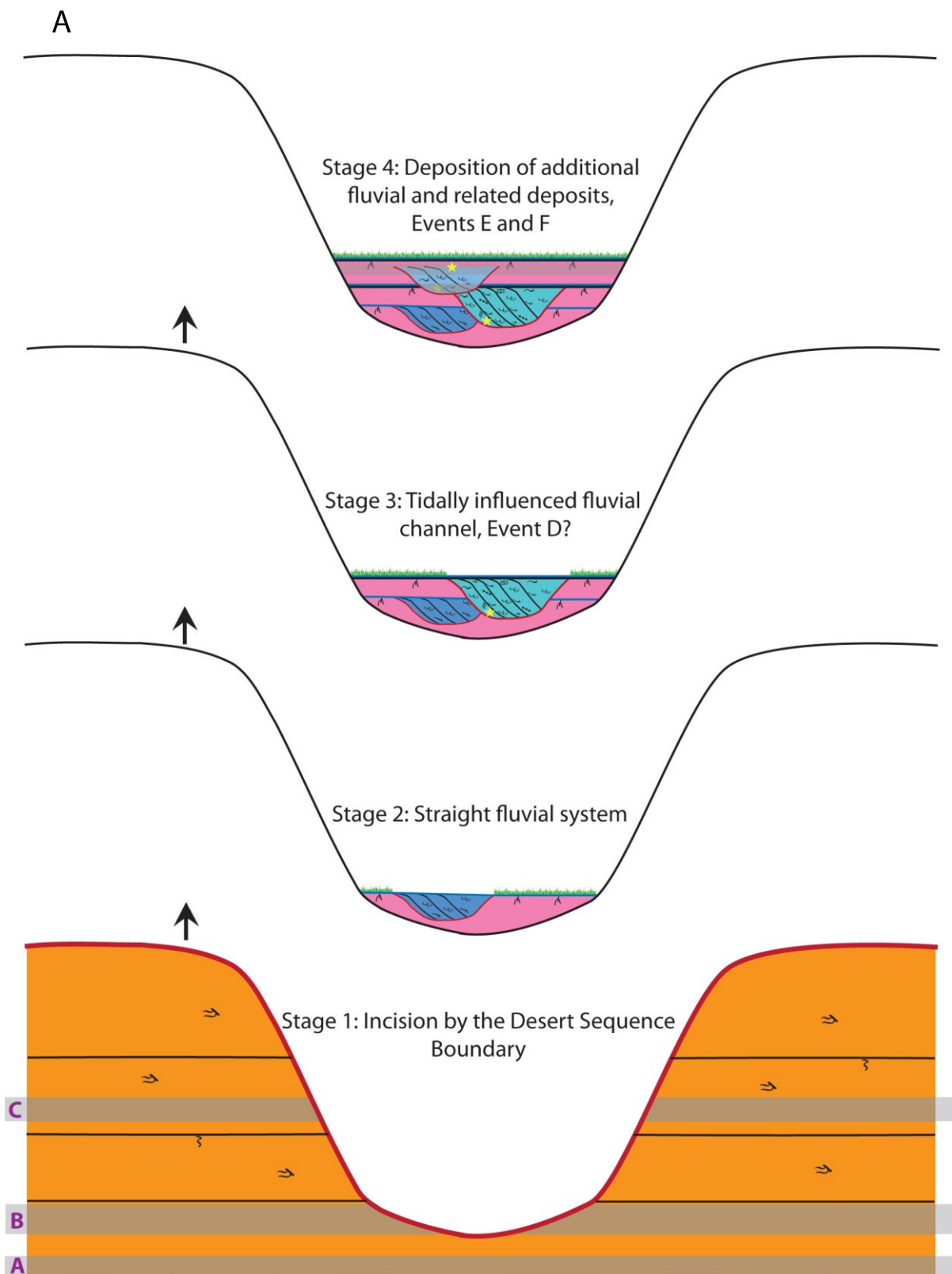
Figure 14a and b. Stages of valley fill within the IVF of the Desert Member. Chemostratigraphic events are represented by a yellow star.

B

Stage 9: Incision by the Castlegate Sequence Boundary

Stage 8: Deposition of overbank deposits and isolated channels

Stage 7: Deposition of a new fluvial channel

Stage 6: New fluvial and overbank deposits, Event H

Stage 5: Deposition of new PS with fluvial and overbank deposits, Event G
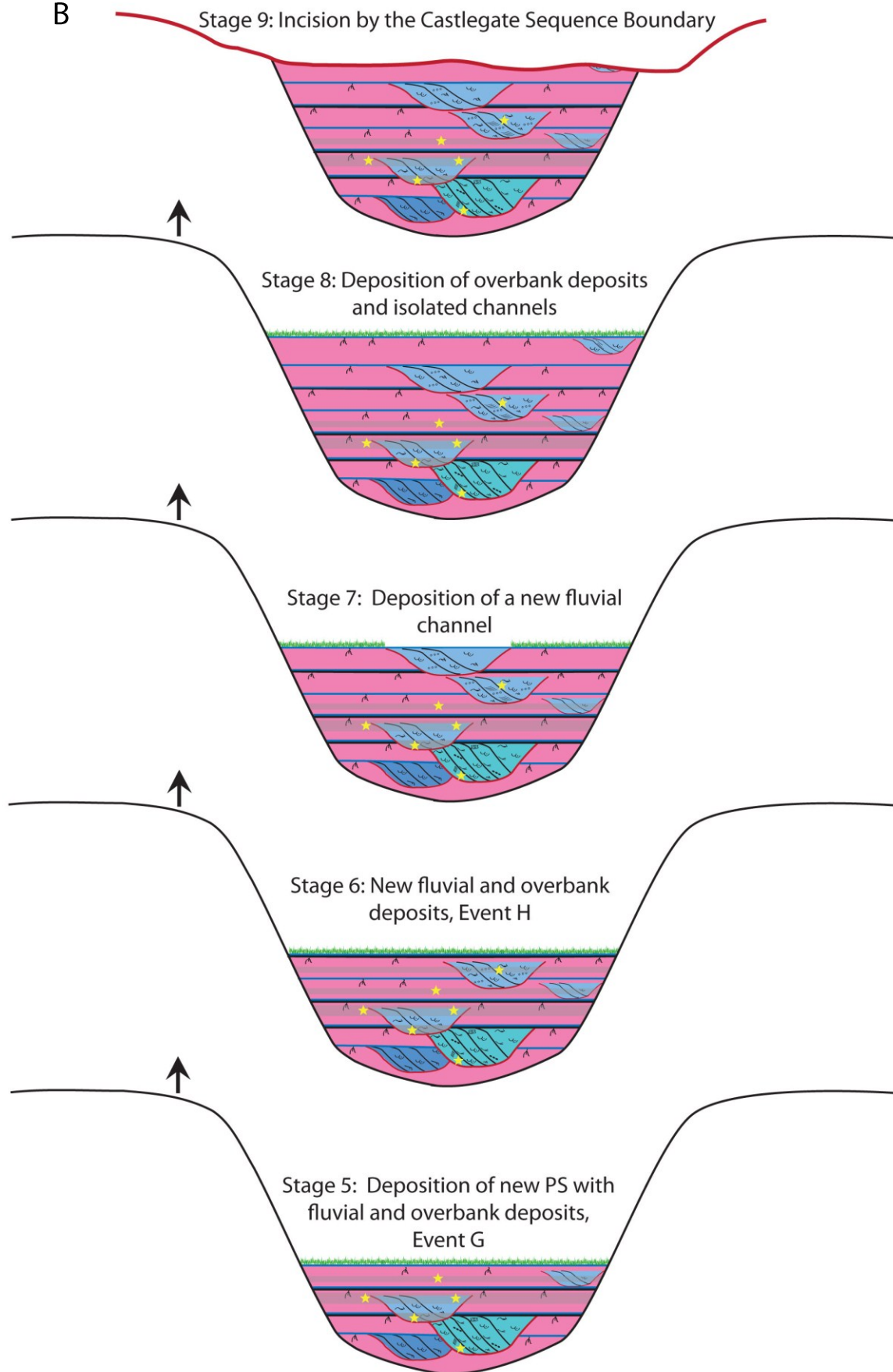
REFERENCES

ATCHLEY, S.C., NORDT, L.C., and DWORKIN, S.I., 2004, Eustatic control on alluvial sequence stratigraphy: A possible example from the Cetaceous-Tertiary transition of the Tornillo basin, Big Bend National Park, West Texas, USA: Journal of Sedimentary Research, v. 74, p. 391-404.

BOUTTON, T.W., ARCHER, S.R., MIDWOOD, A.J., ZITZER, S.F., and BOL, R., 1998, δ^{13}C values of soil organic carbon and their use in documenting vegetation change in a subtropical savanna ecosystem: Geoderma, v. 82, p. 5-41.

BOWN, T.M., and KRAUS, M.J., 1987, Integration of channel and floodplain suites, I. Developmental sequence and lateral relations of alluvial Paleosols: Journal of Sedimentary Research, v. 57, p. 587-601.

BRIDGE, J.S., and LEEDER, M.R., 1979, Simulation-model of alluvial stratigraphy: Sedimentology, v. 26, p. 617-644.

BRIDGE, J.S., and TYE, R.S., 2000, Interpreting the dimensions of ancient fluvial channel bars, channels, and channel belts from wireline-logs and cores: Aapg Bulletin, v. 84, p. 1205-1228.

CERLING, T.E., and QUADE, J., 1993, Stable carbon and oxygen isotopes in soil carbonates, Climate change in continental isotopic records: Geophysical Monograph 78, American Geophysical Union p. 217-231.

CLEVELAND, D.M., ATCHLEY, S.C., and NORDT, L.C., 2007, Continental sequence stratigraphy of the Upper Triassic (Norian–Rhaetian) Chinle strata, northern New Mexico, U.S.A.: allocyclic and autocyclic origins of paleosol-bearing alluvial successions: Journal of Sedimentary Research, v. 77, p. 909-924.

DAVIES, R., DIESSEL, C., HOWELL, J., FLINT, S., and BOYD, R., 2005, Vertical and lateral variation in the petrography of the Upper Cretaceous Sunnyside coal of eastern Utah, USA: implications for the recognition of high-resolution accommodation changes in paralic coal seams: International Journal of Coal Geology, v. 61, p. 13-33.

DIESSEL, C.F., 1992, Coal-bearing depositional systems, Springer-Verlag, Berlin, 721 p.

FOUCH, T.D., LAWTON, T.F., NICHOLS, D.J., CASHION, W.D., and COBBAN, W.A., 1983, Patterns and timing of synorogenic sedimentation in Upper Cretaceous rocks of central and northeast Utah, Mesozoic paleogeography of the west-central United States: Rocky Mountain Paleogeography Symposium, p. 305-336.

GRADSTEIN, F.M., OGG, J.G., SCHMITZ, M.D., OGG, G.M., AGTERBERG, F.P., ANTHONISSEN, D.E., BECKER, T.R., CATT, J.A., COOPER, R.A., DAVYDOV, V.I., GRADSTEIN, S.R., HENDERSON, C.M.,

HILGEN, F.J., HINNOV, L.A., MCARTHUR, J.M., MELCHIN, M.J., NARBONNE, G.M., PAYTAN, A., PENG, S., PEUCKER-EHRENBRINK, B., PILLANS, B., SALTZMAN, M.R., SIMMONS, M.D., SHIELDS, G.A., TANAKA, K.L., VANDENBERGHE, N., VAN KRANENDONK, M.J., ZALASIEWICZ, J., ALTERMANN, W., BABCOCK, L.E., BEARD, B.L., BEU, A.G., BOYES, A.F., CRAMER, B.D., CRUTZEN, P.J., VAN DAM, J.A., GEHLING, J.G., GIBBARD, P.L., GRAY, E.T., HAMMER, O., HARTMANN, W.K., HILL, A.C., HOFFMAN, P.F., HOLLIS, C.J., HOOKER, J.J., HOWARTH, R.J., HUANG, C., JOHNSON, C.M., KASTING, J.F., KERP, H., KORN, D., KRIJGSMAN, W., LOURENS, L.J., MACGABHANN, B.A., MASLIN, M.A., MELEZHIK, V.A., NUTMAN, A.P., PAPINEAU, D., PILLER, W.E., PIRAJNO, F., RAVIZZA, G.E., SADLER, P.M., SPEIJER, R.P., STEFFEN, W., THOMAS, E., WARDLAW, B.R., WILSON, D.S., and XIAO, S., 2012, The Geologic Time Scale 2012: Boston, USA.

HAMPSON, G.J., DAVIES, W., DAVIES, S.J., HOWELL, J.A., and ADAMSON, K.R., 2005, Use of spectral gamma-ray data to refine subsurface fluvial stratigraphy: Late Cretaceous strata in the Book Cliffs, Utah, USA: Journal of the Geological Society, v. 162, p. 603-621.

HÄNTZSCHEL, W., 1962, Trace fossils and problematica, *in* Hass, W.H., Hantzschel, W., Fisher, D.W., Howell, B.F., Rhodes, F.H.T., Müller, K.J., and Moore, R.C., eds., Treatise on invertebrate paleontology: Pt. W, Miscellanea: The University of Kansas and GSA, Lawrence, KS, p. W177-W245.

HILDRED, G.V., RATCLIFFE, K.T., WRIGHT, A.M., ZAITLIN, B.A., and WRAY, D.S., 2010, Chemostratigraphic applications to low-accomodation fluvial valley settings: an example from the lower Mannville Formation of Alberta, Canada Journal of Sedimentary Research, v. 80, p. 1032-1045.

HOFFMEISTER, K.E., 2011, Forebulge influence on deposition of the Cretaceous Castlegate Sandstone, Book Cliffs, Utah, U.S.A.: The University of Kansas, Dissertation Publishing, 107 p.

HOUSTON, W.S., HUNTOON, J.E., and KAMOLA, D.L., 2000, Modeling of Cretaceous foreland-basin parasequences, Utah, with implications for timing of Sevier thrusting: Geology, v. 28, p. 267-270.

HUBER, B.T., NORRIS, R.D., and MACLEOD, K.G., 2002, Deep-sea paleotemperature record of extreme warmth during the Cretaceous: Geology, v. 30, p. 123-126.

JARVIS, I., GALE, A.S., JENKYNS, H.C., and PEARCE, M.A., 2006, Secular variation in Late Cretaceous carbon isotopes: a new $\delta^{13}C$carbonate reference curve for the Cenomanian-Campanian (99.6-70.6 Ma): Geological Magazine, v. 143, p. 561-608.

JARVIS, I., MABROUK, A., MOODY, R.T.J., and DE CABRERA, S., 2002, Late Cretaceous (Campanian) carbon isotope events, sea-level change and correlation of the Tethyan and Boreal realms: Palaeogeography Palaeoclimatology Palaeoecology, v. 188, p. 215-248.

JENKYNS, H.C., GALE, A.S., and CORFIELD, R.M., 1994, Carbon- and oxygen-isotope stratigraphy of the English Chalk and Italian Scaglia and its palaeoclimate significance: Geological Magazine, v. 131, p. 1-34.

JORDAN, T.E., 1981, Thrust loads and foreland basin evolution, Cretaceous, western United States: The AAPG Bulletin, v. 65, p. 2506-2520.

KAUFFMAN, E.G., 1977, Geological and biological overview; Western Interior Cretaceous basin, *in* Kauffman, E.G., ed., Cretaceous facies, faunas, and paleoenvironments across the Western Interior Basin: The Mountain Geologist Rocky Mountain Association of Geologists, p. 75-99.

KRAUS, M.J., 1987, Integration of channel and floodplain suites, II. Vertical relations of alluvial Paleosols: Journal of Sedimentary Research, v. 57, p. 602-612.

KRAUS, M.J., 1999, Paleosols in clastic sedimentary rocks: their geologic applications: Earth-Science Reviews, v. 47, p. 41-70.

LOTTES, A.L., and ZIEGLER, A.M., 1994, World peat occurrence and the seasonality of climate and vegetation: Palaeogeography, Palaeoclimatology, Palaeoecology, v. 106, p. 23-37.

MACK, G.H., JAMES, W.C., and MONGER, H.C., 1993, Classification of paleosols: Geological Society of America Bulletin, v. 105, p. 129-136.

MIALL, A.D., 1996, The geology of fluvial deposits; sedimentary facies, basin analysis, and petroleum geology: Federal Republic of Germany, Springer-Verlag : Berlin, Federal Republic of Germany, 582 p.

MYER, M., 2012, Unpublished work, The University of Kansas.

OBRADOVICH, J.D., 1993, A Cretaceous time scale, *in* Caldwell, W.E.G., and Kauffman, E.G., eds., Evolution of the Western Interior Basin: Geological Association of Canada, p. 379-398.

PARKER, L.R., 1976, The paleoecology of the fluvial coal-forming swamps and associated floodplain environments in the Blackhawk Formation (Upper Cretaceous) of central Utah: BYU Geology Studies, v. 22, Part 3, p. 99-116.

RETALLACK, G., 1984, Completeness of the rock and fossil record: some estimates using fossil soils: Paleobiology, v. 10, p. 59-78.

RETALLACK, G.J., 1988, Field recognition of paleosols *in* Reinhardt, J., and Sigleo, W.R., eds., Paleosols and weathering through geologic time: principles and applications: Special Paper 216, Geological Society of America, p. 1-20.

RETALLACK, G.J., 1990, Soils of the past: an introduction to paleopedology, Unwin Hyman, Boston, MA, 520 p.

RETALLACK, G.J., 1998, Fossil soils and completeness of the rock and fossil records, *in* Donovan, P., Stephen K., Christopher R. C., ed., The adequacy of the fossil record, John Wiley & Sons, Chichester, United Kingdom, p. 133-163.

SCHEPPY, R., 2000, A three-dimenstional analysis of the internal architecture of an incised valley: Desert Member, Blackhawk Formation, Book Cliffs, Utah: The University of Kansas 166 p.

SHANLEY, K.W., MCCABE, P.J., and HETTINGER, R.D., 1992, Tidal influence in Cretaceous fluvial strata from Utah, USA: a key to sequence stratigraphic interpretation: Sedimentology, v. 39, p. 905-930.

SOIL SURVEY STAFF, 2010, Keys to soil taxonomy, Eleventh Edition, USDA Natural Resources Conservation Service, Washington, D.C., 338 p.

VAN WAGONER, J.C., 1995, Sequence stratigraphy and marine to nonmarine facies architecture of foreland basin strata, Book Cliffs, Utah, U.S.A. , *in* Van Wagoner, J.C., and Bertram, G.T., eds., Sequence stratigraphy of foreland basin deposits; outcrop and subsurface examples from the Cretaceous of North America AAPG Memoir 64, p. 137-223.
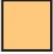
VAN WAGONER, J.C., MITCHUM, R.M., CAMPION, K.M., and RAHMANIAN, V.D., 1990, Siliciclastic sequence stratigraphy in well logs, cores, and outcrops; concepts for high-resolution correlation of time and facies: Methods in Exploration Series, v. 7, 755 p.

VAN WAGONER, J.C., POSAMENTIER, H.W., MITCHUM, R.M., VAIL, P.R., SARG, J.F., LOUTIT, T.S., and HARDENBOL, J., 1988, An overview of sequence stratigraphy and key definitions, *in* Wilgus, C., Hastings, B.S., Kendall, C.G., Posamentier, H.W., Ross, C.A., and Van Wagoner, J.C., eds., Sea level changes: an integradted approach: SEPM Special Publication, p. 39-45.

WRIGHT, V.P., and MARRIOTT, S.B., 1993, The sequence stratigraphy of fluvial depositional systems: the role of floodplain sediment storage: Sedimentary Geology, v. 86, p. 203-210.

Key

Interbedded HCS and Siltstone	Tidally Influenced Fluvial System	Coal	Straight Fluvial System
Amalgamated HCS	Sinuous Fluvial System	Overbank	Chemostratigraphic Event
Sequence Boundary	Mega ripples	Wood clast	*Schab cylindrichnus*
Flooding Surface	Wave ripple	Rooting	*Diplocurterian*
Datum	Lamination	Plant debris	*Teredolites*
HCS	Soft sediment deformation	Platy peds	*Treptichnus*
Trough crossbeds	Mud clasts	Blocky peds	*Conicnus*
Wedge crossbeds	Shell lag	Bioturbation	*Chondrites*
Planar Tabular crossbeds	Rip up clasts	*Macronichnus*	*Thalassanoides*
Reactivation surface	Mud drape	Paleophycus	Paleosol
Flaser bedding	Double mud drape	*Taednidium*	
Current ripple	Mottling	*Aulichnites*	

Tuscher 1 Measured Section
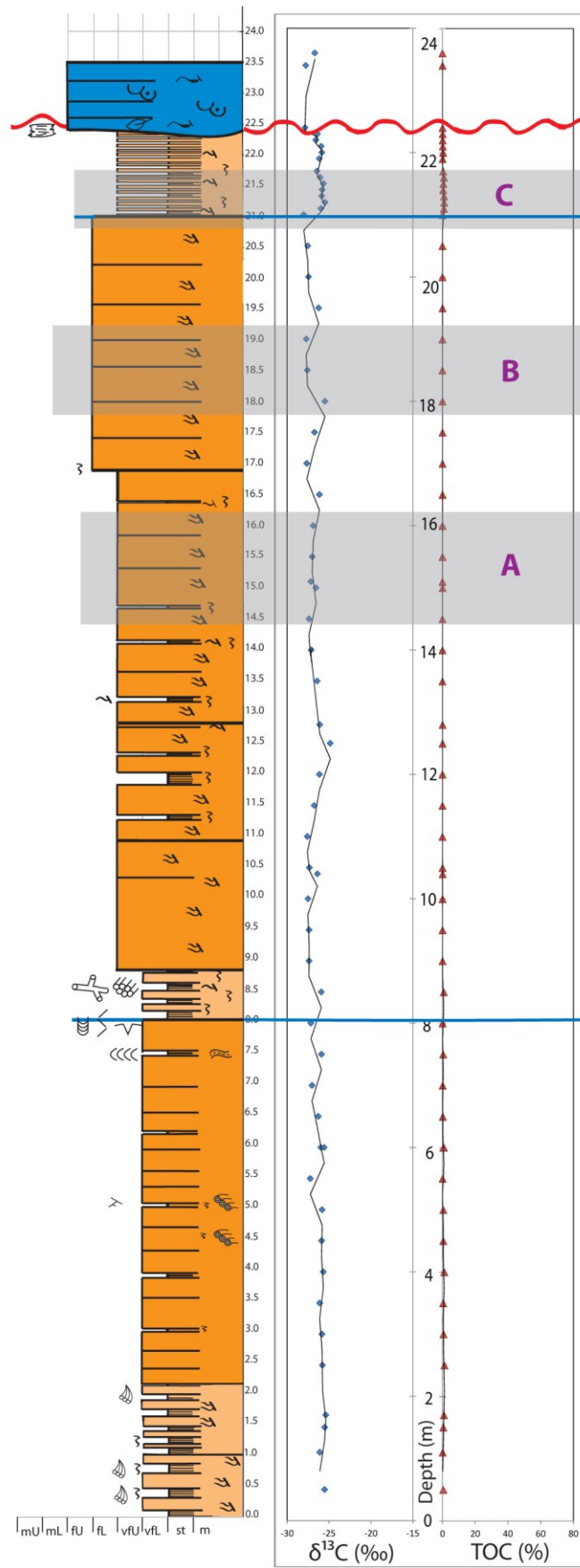
Tuscher 2 Measured Section

52
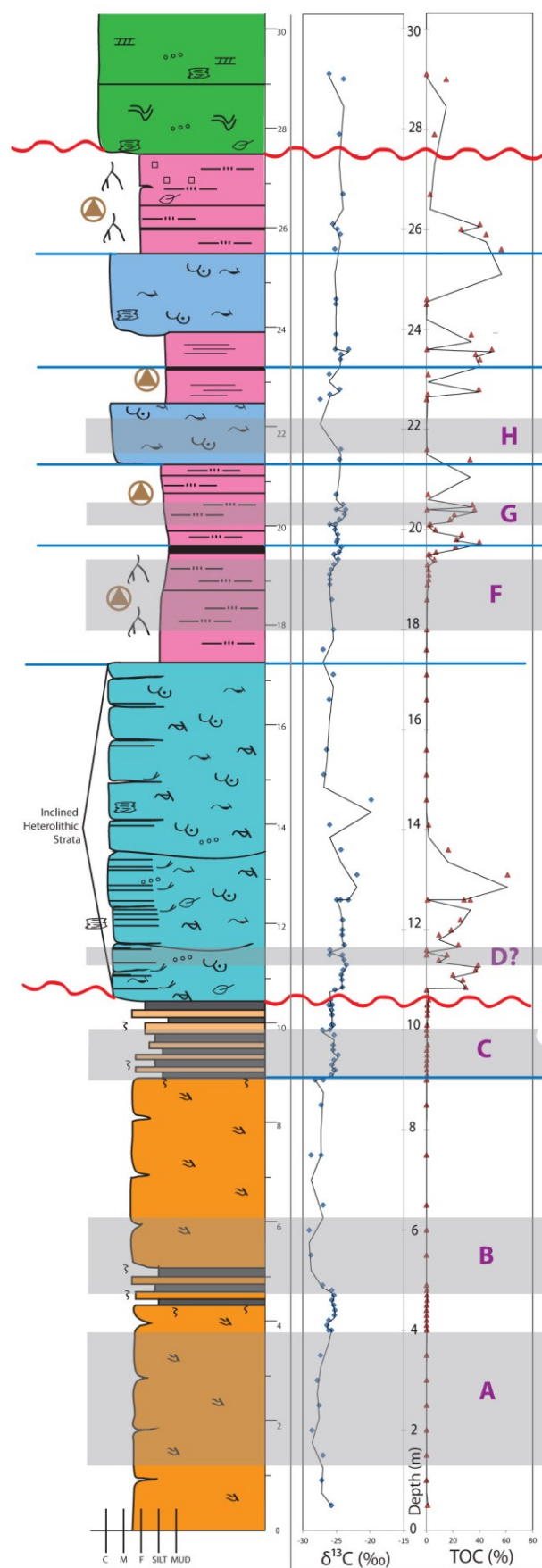
Tuscher 3 Measured Section

53
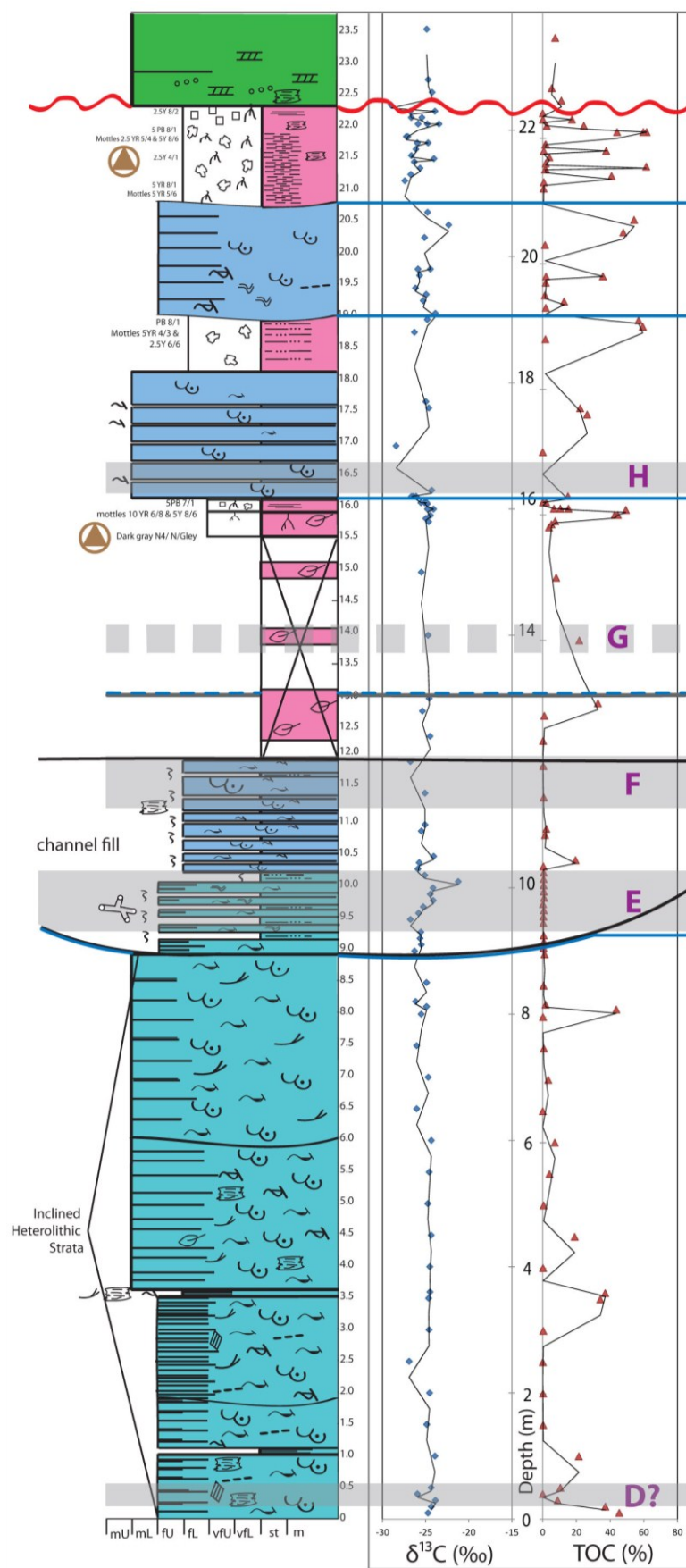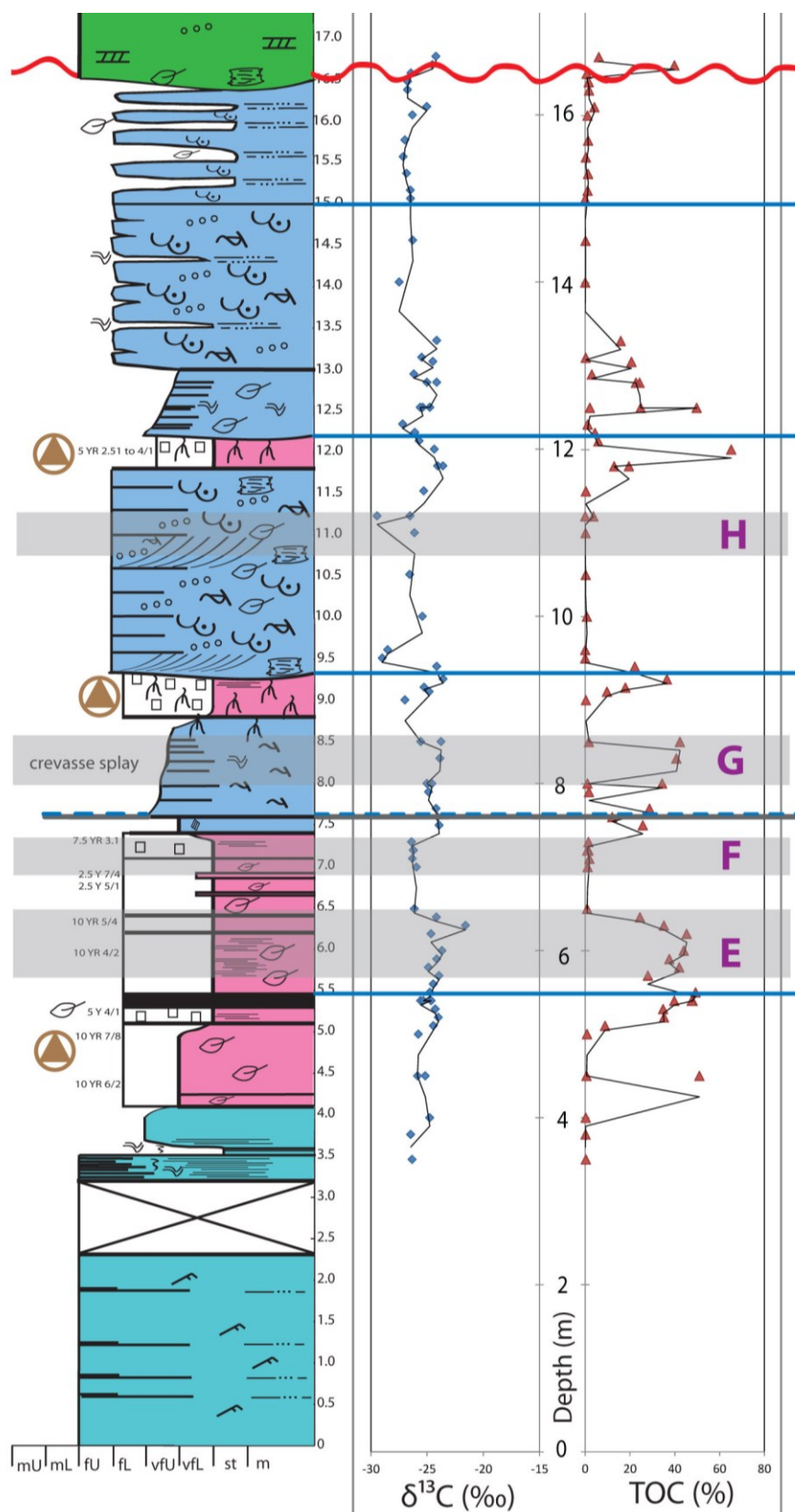
Stable Isotope Percent Carbonate
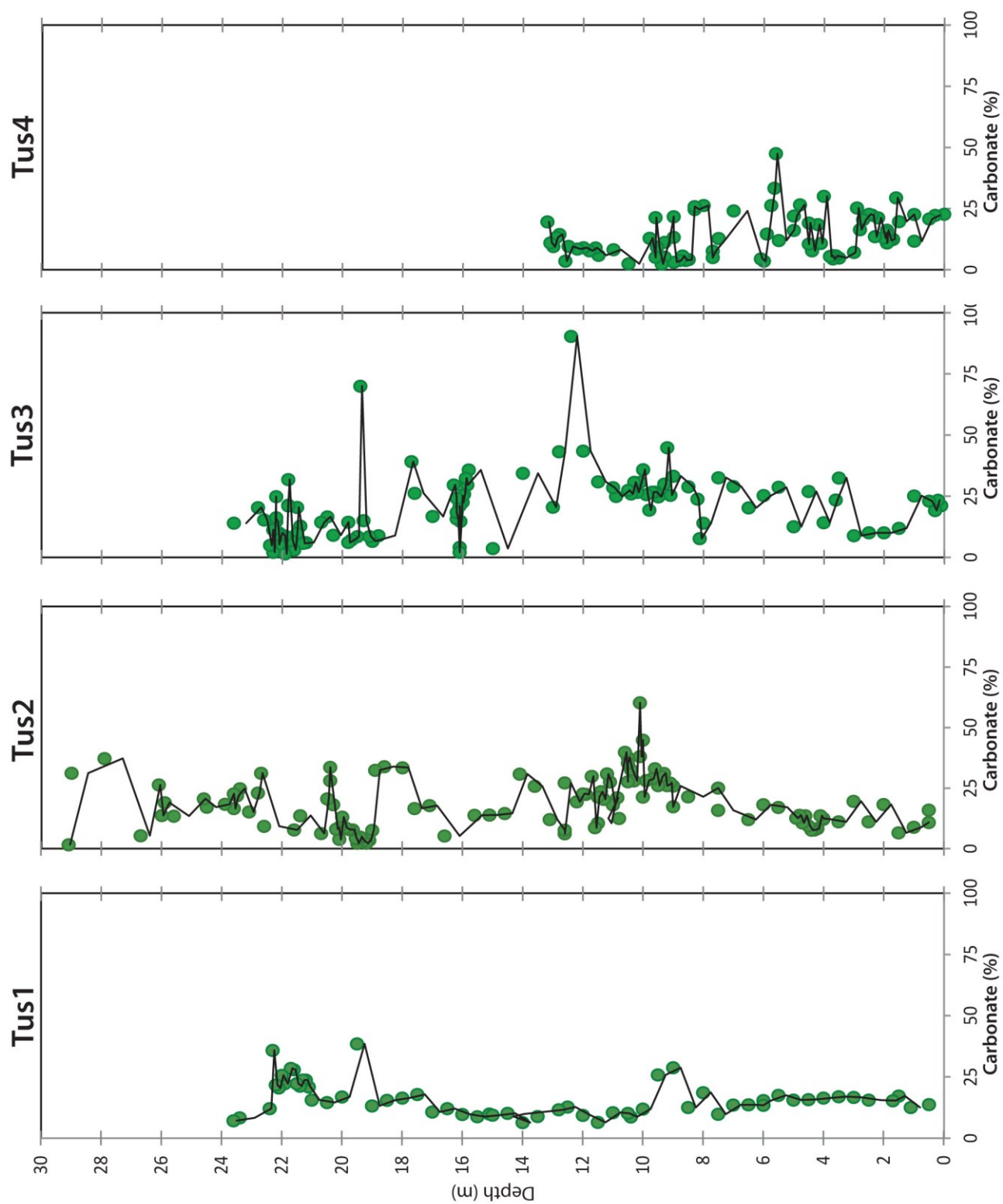
Tuscher 1 Stable Isotope Data

Sample Number	Depth (m)	Percent Carbonate (%)	TOC (%)	$\delta^{13}C_{org}$ (‰)
TUS1-0.5 H	0.5	13.8	0.51	-25.52
TUS1-1.1 H	1.1	12.5	0.18	-26.09
TUS1-1.5 H	1.5	17.2	0.54	-25.51
TUS1-1.7 H	1.7	15.3	0.89	-25.37
TUS1-2.5 H	2.5	15.5	1.27	-25.77
TUS1-3.0 H	3.0	16.7	0.69	-25.83
TUS1-3.5 H	3.5	17.0	0.49	-26.10
TUS1-4.0 H	4.0	16.4	1.10	-25.67
TUS1-4.5 H	4.5	15.8	0.50	-25.88
TUS1-5.0 H	5.0	15.6	0.54	-25.82
TUS1-5.5 H	5.5	17.5	0.09	-27.23
TUS1-6.0 H	6.0	15.4	0.93	-25.57
TUS1-6.5 H	6.0	13.6	0.25	-26.28
TUS1-7.0 H	6.5	13.6	0.20	-27.02
TUS1-7.5 H	7.0	9.8	0.48	-25.89
TUS1-8.0 H	7.5	18.7	0.11	-27.15
TUS1-8.5 H	8.0	12.6	0.81	-25.92
TUS1-9.0 H	8.5	28.8	0.11	-27.37
TUS1-9.5 H	9.0	25.8	0.08	-27.37
TUS1-10.0 H	9.5	11.9	0.08	-27.51
TUS1-10.4 H	10.0	8.7	0.15	-26.38
TUS1-10.5 H	10.4	10.1	0.10	-27.33
TUS2-11.0 H	10.5	10.5	0.06	-27.58
TUS2-11.5 H	11.0	6.5	0.06	-26.76
TUS2-12.0 H	11.5	9.4	0.05	-26.13
TUS2-12.5 H	12.0	12.8	0.08	-24.84
TUS2-12.8 H	12.5	11.6	0.06	-26.09
TUS2-15.1 H	12.8	9.9	0.03	-27.16
TUS3-13.5 H	15.1	8.8	0.05	-26.40
TUS3-14.0 H	13.5	6.4	0.06	-27.12
TUS3-14.5 H	14.0	10.1	0.05	-27.37
TUS3-15.0 H	14.5	9.4	0.08	-26.54
TUS3-15.5 H	15.0	8.8	0.05	-26.99
TUS3-16.0 H	15.5	9.7	0.05	-26.87
TUS3-16.5 H	16.0	12.1	0.11	-26.13
TUS3-17.0 H	16.5	10.7	0.06	-27.64
TUS3-17.5 H	17.0	17.8	0.10	-26.72
TUS3-18.0 H	17.5	16.4	0.05	-25.48
TUS3-18.5 RH	18.0	15.5	0.04	-27.57
TUS3-19.0 H	18.5	13.2	0.05	-27.70
TUS3-19.5 H	19.0	38.5	0.11	-26.23

TUS3-20.0 H	19.5	16.8	0.03	-27.42
TUS3-20.5 H	20.0	14.6	0.05	-27.53
TUS3-21.0 H	20.5	15.6	0.06	-28.00
TUS3-21.1 H	21.0	20.9	0.93	-25.95
TUS3-21.2 H	21.1	23.8	1.07	-25.47
TUS3-21.3 H	21.2	23.7	1.04	-25.86
TUS3-21.4 H	21.3	21.3	0.47	-25.81
TUS3-21.5 H	21.4	22.3	0.65	-25.66
TUS3-21.6 H	21.5	28.0	0.89	-26.04
TUS3-21.7 H	21.6	28.5	0.50	-26.43
TUS3-21.9 H	21.7	22.2	0.15	-26.14
TUS3-22.0 H	21.9	25.7	0.38	-25.85
TUS3-22.1 H	22.0	20.5	0.22	-25.92
TUS3-22.2 H	22.1	21.7	0.14	-26.56
TUS3-22.3 H	22.2	35.9	0.15	-26.37
TUS3-22.4 H	22.3	12.1	0.08	-27.85
TUS3-23.4 RH	22.4	8.3	0.07	-27.75
TUS3-23.6 H	23.4	7.2	0.05	-26.68

Tuscher 2 Stable Isotope Data

Sample Number	Depth (m)	Percent Carbonate (%)	TOC (%)	$\delta^{13}C_{org}$ (‰)
TUT-0.5	0.5	16.0	0.92	-25.73
TUT-0.5R	0.5	10.9	1.01	-25.79
TUT-1.0	1.0	8.9	0.05	-27.20
TUT-1.5	1.5	6.6	0.07	-27.01
TUT-2.0	2.0	18.3	0.10	-28.65
TUT-2.5	2.5	11.1	0.07	-27.58
TUT-3.0	3.0	19.6	0.10	-27.86
TUT-3.5	3.5	11.1	0.07	-27.38
TUT-4.0	4.0	12.1	0.18	-26.15
TUT-4.0R	4.0	12.5	0.36	-25.73
TUT-4.1	4.1	13.7	0.12	-26.43
TUT-4.2	4.2	8.4	0.09	-26.15
TUT-4.3	4.3	7.8	0.09	-25.32
TUT-4.4	4.4	7.7	0.05	-25.23
TUT-4.5	4.5	9.4	0.16	-25.42
TUT-4.6	4.6	13.6	0.51	-25.68
TUT-4.7	4.7	10.6	0.32	-25.38
TUT-4.8	4.8	13.8	0.34	-25.69
TUT-4.9	4.9	12.6	0.09	-27.07
TUT-5.5	5.5	17.1	0.06	-28.80
TUT-6.0	6.0	18.1	0.07	-29.07
TUT-6.5	6.5	12.1	0.04	-26.98
TUT-7.5	7.5	15.8	0.05	-28.79
TUT-7.5R	7.5	25.1	0.05	-27.29
TUT-8.5	8.5	21.4	0.06	-27.32
TUT-9.0	9.0	25.9	0.24	-26.94
TUT-9.0R	9.0	17.3	0.04	-28.18
TUT-9.1	9.1	27.1	0.53	-25.78
TUT-9.2	9.2	26.2	0.25	-25.36
TUT-9.2R	9.2	26.1	0.20	-25.19
TUT-9.3	9.3	31.1	0.14	-25.68
TUT-9.4	9.4	29.8	0.42	-25.39
TUT-9.5	9.5	26.1	0.53	-24.76
TUT-9.6	9.6	33.0	0.22	-25.50
TUT-9.7	9.7	28.9	0.94	-25.51
TUT-9.9	9.9	28.2	0.42	-25.35
TUT-10.0	10.0	21.4	0.14	-27.07
TUT-10.0R	10.0	44.8	0.23	-26.01
TUT-10.1	10.1	38.0	0.58	-25.52
TUT-10.1R	10.1	60.3	0.40	-25.74
TUT-10.3	10.3	28.0	0.78	-25.66

TUT-10.4	10.4	32.7	0.89	-25.71
TUT-10.5	10.5	37.7	0.92	-26.17
TUT-10.5R	10.5	35.4	1.02	-25.62
TUT-10.5RR	10.5	27.7	0.54	-25.77
TUT-10.6	10.6	39.9	1.66	-25.89
C-0.2	10.8	12.5	0.17	-25.23
C-0.25	10.9	21.0	29.54	-24.11
C-0.4	11.0	18.1	27.32	-24.18
C-0.5	11.1	27.5	19.89	-24.29
C-0.6	11.2	30.9	36.90	-24.02
C-0.7	11.3	20.4	38.80	-23.53
C-0.8	11.4	23.5	9.34	-23.89
C-0.9	11.5	21.4	15.50	-24.10
C-1.0	11.6	8.7	0.11	-25.99
C-1.1	11.7	29.9	24.06	-23.85
C-1.3	11.9	22.5	9.48	-24.16
C-1.4	12.0	22.7	18.67	-24.14
C-1.6	12.2	19.4	25.51	-24.09
C-2.0	12.6	27.2	33.05	-24.41
C-2.0R	12.6	6.2	0.87	-24.97
C-2.0RR	12.6	7.7	28.28	-23.23
C-2.5	13.1	12.0	61.09	-21.96
C-3.0	13.6	25.8	16.49	-24.34
C-3.5	14.1	30.9	1.69	-26.02
C-4.0	14.6	14.6	0.03	-19.84
C-4.5	15.1	13.9	0.06	-26.88
C-5.0	15.6	13.8	0.02	-26.46
C-6.0	16.6	5.3	0.15	-26.09
C-6.5	17.1	17.8	0.16	-25.47
C-7.0	17.6	16.6	0.03	-26.99
C-7.4	18.0	33.4	0.29	-25.45
C-8.0	18.6	33.9	0.37	-25.70
C-8.3	18.9	32.4	0.75	-25.98
C-8.4	19.0	7.6	1.67	-25.97
C-8.5	19.1	3.5	1.81	-26.02
C-8.6	19.2	2.3	1.53	-25.79
C-8.7	19.3	3.1	0.80	-25.40
C-8.8	19.4	4.8	6.03	-24.77
C-8.9	19.5	2.3	1.48	-25.38
C-8.9R	19.5	3.9	2.56	-25.33
C-8.95	19.6	4.3	7.17	-24.60
C-9.05	19.7	7.8	21.99	-24.26
C-9.15	19.8	7.9	39.89	-25.00
C-9.2	19.8	8.1	22.52	-24.85
C-9.3	19.9	8.7	26.66	-24.83

C-9.4	20.0	13.1	6.66	-25.24
C-9.5	20.1	3.8	2.20	-25.13
C-9.5	20.1	8.8	3.18	-26.01
C-9.6	20.2	8.1	17.79	-24.56
C-9.7	20.3	18.2	20.99	-23.82
C-9.8	20.4	28.1	36.26	-23.64
C-9.8R	20.4	33.6	0.44	-25.05
C-9.9	20.5	20.6	34.69	-24.05
C-10.1	20.7	6.3	1.18	-25.06
C-10.8	21.4	13.7	32.83	-24.57
C-11.0	21.6	7.8	0.39	-24.35
C-12.0	22.6	9.3	0.09	-27.42
C-12.1	22.7	31.2	0.95	-25.99
C-12.2	22.8	23.0	39.47	-24.52
C-12.5	23.1	15.2	1.23	-26.09
C-12.8	23.4	24.8	40.20	-24.44
C-12.9	23.5	21.9	37.06	-24.34
C-13.0	23.6	16.6	49.28	-23.18
C-13.0R	23.6	22.7	0.53	-25.16
C-13.3	23.9	18.3	33.79	-25.08
C-13.9	24.5	17.2	0.09	-25.11
C-14.0	24.6	20.6	0.24	-25.05
C-15.0	25.6	13.5	56.43	-25.25
C-15.3	25.9	19.0	44.97	-24.43
C-15.4	26.0	13.7	26.16	-24.86
C-15.5	26.1	26.4	40.34	-25.53
C-16.1	26.7	5.4	2.74	-24.03
C-17.3	27.9	37.3	6.09	-24.58
C-18.4	29.0	31.2	14.95	-23.95
C-18.5	29.1	1.7	0.08	-26.09

Tuscher 3 Stable Isotope Data

Sample Number	Depth (m)	Percent Carbonate (%)	TOC (%)	$\delta^{13}C_{org}$ (‰)
Tus3c-0.1 V	0.1	21.2	0.51	-24.71
Tus3c-0.2 V	0.2	23.4	0.18	-24.33
Tus3c-0.3 V	0.3	19.2	0.54	-23.85
Tus3c-0.4 H	0.4	0.0	0.89	-25.93
Tus3c-0.5 V	0.5	23.0	1.27	-24.34
Tus3c-1.0 V	1.0	25.2	0.69	-23.91
Tus3c-1.5 H	1.5	11.9	0.49	-24.86
Tus3c-2.0 H	2.0	10.1	1.10	-24.54
Tus3c-2.5 H	2.5	10.1	0.50	-26.91
Tus3c-3.0 H	3.0	8.9	0.54	-24.59
Tus3c-3.5 V	3.5	32.5	0.09	-24.64
Tus3c-3.6 V	3.6	23.5	0.93	-24.49
Tus3c-4.0 H	4.0	14.2	0.51	-24.51
Tus3c-4.5 V	4.5	27.0	0.25	-24.35
Tus3c-5.0 H	5.0	12.5	0.20	-24.73
Tus3c-5.5 V	5.5	28.7	0.48	-24.57
Tus3c-6.0 H	6.0	25.3	0.11	-24.34
Tus3c-6.5 H	6.5	20.3	0.81	-26.02
Tus3c-7.0 V	7.0	29.0	0.11	-24.69
Tus3c-7.5 V	7.5	32.6	0.08	-26.01
Tus3c-8.0 H	8.0	14.0	0.08	-25.49
Tus3c-8.12 V	8.1	7.7	0.15	-24.89
Tus3c-8.2 H	8.2	23.8	0.10	-26.15
Tus3c-8.5 V	8.5	28.9	0.06	-24.89
Tus3c-9.0 V	9.0	33.2	0.06	-26.27
Tus3c-9.1 V	9.1	25.4	0.05	-25.49
Tus3c-9.2 V	9.2	44.8	0.08	-25.62
Tus3c-9.3 V	9.3	30.0	0.06	-25.54
Tus3c-9.5 H	9.5	24.7	0.03	-26.74
Tus3c-9.6 H	9.6	26.7	0.05	-25.79
Tus3c-9.7 V	9.7	26.7	0.06	-25.26
Tus3c-9.8 H	9.8	19.3	0.05	-24.11
Tus3c-9.9 V	9.9	25.7	0.08	-24.44
Tus3c-10.0 H	10.0	35.9	0.05	-24.14
Tus3c-10.1 V	10.1	30.8	0.05	-21.22
Tus3c-10.2 V	10.2	26.6	0.11	-25.08
Tus3c-10.3 V	10.3	30.7	0.06	-25.88
Tus3c-10.4 V	10.4	25.9	0.10	-25.72
Tus3c-10.5 V	10.5	27.4	0.05	-24.06
Tus3c-10.9 V	10.9	24.9	0.04	-25.49
Tus3c-11.0 V	11.0	28.5	0.05	-25.06

Tus3c-11.5 H	11.5	30.9	0.11	-25.06
Tus3c-12.0 H	12.0	43.5	0.03	-26.74
Tus3c-12.4 V	12.4	90.3	0.05	-24.47
Tus3c-12.8B V	12.8	43.2	0.06	-25.36
Tus3c-13.0 V	13.0	20.5	0.93	-24.57
Tus3c-14.0 V	14.0	34.3	1.07	-24.70
Tus3c-15.0 H	15.0	3.6	1.04	-25.48
Tus3c-15.8 V	15.8	35.8	0.47	-24.65
Tus3c-15.85 V	15.9	29.6	0.65	-24.96
Tus3c-15.9 Root V	15.9	32.4	0.89	-24.43
Tus3c-16.0 V	16.0	22.5	0.15	-24.77
Tus3c-16.0R V	16.0	25.2	0.38	-24.07
Tus3c-16.08 V	16.1	14.8	0.22	-24.81
Tus3c-16.1 H	16.1	4.1	0.14	-25.10
Tus3c-16.1 V	16.1	21.1	0.15	-24.88
Tus3c-16.1 H	16.1	2.1	0.08	-25.52
Tus3c-16.2 H	16.2	15.7	0.07	-26.09
Tus3c-16.2 H	16.2	18.4	0.05	-26.43
Tus3c-16.2 V	16.2	24.2	45.44	-26.62
Tus3c-16.3 V	16.3	29.6	37.18	-24.28
Tus3c-17.0 H	17.0	16.7	8.90	-28.40
Tus3c-17.6 V	17.6	26.2	0.06	-24.62
Tus3c-17.7 V	17.7	39.2	10.52	-24.96
Tus3c-18.8 H	18.8	8.9	21.49	-26.27
Tus3c-19.0 V	19.0	6.6	0.25	-24.79
Tus3c-19.1 V	19.1	8.5	0.17	-23.85
Tus3c-19.3 V	19.3	15.0	0.05	-25.27
Tus3c-19.4 V	19.4	70.0	0.33	-24.91
Tus3c-19.5 H	19.5	8.5	34.19	-26.15
Tus3c-19.7 H	19.7	7.2	37.10	-25.67
Tus3c-19.8 H	19.8	6.1	0.20	-25.86
Tus3c-19.8 V	19.8	14.4	18.95	-24.43
Tus3c-20.3 H	20.3	9.1	0.55	-25.11
Tus3c-20.5 RV	20.5	16.6	4.04	-22.32
Tus3c-20.7 V	20.7	14.4	7.24	-24.76
Tus3c-21.2 H	21.2	6.1	0.02	-27.40
Tus3c-21.3 H	21.3	5.8	3.27	-26.70
Tus3c-21.4 V	21.4	12.9	0.66	-25.62
Tus3c-21.5 H	21.5	20.5	0.18	-26.27
Tus3c-21.5 RH	21.5	9.9	43.60	-26.31
Tus3c-21.55 V	21.6	-1.8	1.70	-24.02
Tus3c-21.6 H	21.6	3.0	0.48	-26.64
Tus3c-21.7 H	21.7	6.9	1.14	-26.11
Tus3c-21.8 H	21.8	31.9	0.49	-25.95
Tus3c-21.8 V	21.8	21.1	0.57	-24.70

Tus3c-21.9 CH	21.9	1.5	0.35	-27.23
Tus3c-21.9 RH	21.9	8.8	0.41	-27.06
Tus3c-22.1 H	22.1	10.0	0.68	-25.85
Tus3c-22.1 V	22.1	5.3	0.19	-23.42
Tus3c-22.1 V	22.1	9.1	0.80	-24.79
Tus3c-22.2 V	22.2	14.6	0.69	-25.41
Tus3c-22.2 RH	22.2	16.2	0.53	-26.65
Tus3c-22.3 H	22.3	2.1	0.60	-26.77
Tus3c-22.3 V	22.3	11.3	0.42	-23.92
Tus3c-22.4 H	22.4	4.9	19.50	-28.98
Tus3c-22.6 V	22.6	15.3	1.39	-24.23
Tus3c-22.8 V	22.8	20.4	2.12	-24.68
Tus3c-23.6R V	23.6	14.0	0.63	-24.86

Tuscher 4 Stable Isotope Data

Sample Number	Depth (m)	Percent Carbonate (%)	TOC (%)	$\delta^{13}C_{org}$ (‰)
Tus4-3.5 H	3.5	22.8	0.31	-26.33
Tus4-3.8 H	3.8	22.2	0.16	-26.46
Tus4-4.0 H	4.0	20.8	0.24	-24.77
Tus4-4.5 RV	4.5	11.7	50.96	-25.16
Tus4-4.5 H	4.5	22.6	0.60	-25.85
Tus4-5.0 H	5.0	19.7	0.80	-25.78
Tus4-5.1 V	5.1	29.4	8.90	-24.44
Tus4-5.2 V	5.2	12.5	35.20	-24.00
Tus4-5.3 V	5.3	12.0	34.81	-24.28
Tus4-5.4 H	5.4	16.2	39.78	-25.58
Tus4-5.4 V	5.4	11.0	48.00	-24.64
Tus4-5.4 RV	5.4	15.1	47.53	-25.34
Tus4-5.5 V	5.5	13.0	49.27	-24.75
Tus4-5.6 V	5.6	-196.7	109.91	-24.46
Tus4-5.7 V	5.7	21.2	27.99	-23.95
Tus4-5.8 V	5.8	13.5	42.00	-24.89
Tus4-5.9 V	5.9	22.3	37.58	-24.15
Tus4-6.0 V	6.0	22.7	44.01	-23.67
Tus4-6.2 V	6.2	20.5	45.29	-24.66
Tus4-6.3 V	6.3	16.4	35.16	-21.58
Tus4-6.4 V	6.4	25.3	24.43	-24.18
Tus4-6.5 H	6.5	7.1	0.87	-26.14
Tus4-7.0 H	7.0	4.9	1.09	-25.95
Tus4-7.1 H	7.1	5.7	1.88	-26.31
Tus4-7.2 H	7.2	4.5	1.48	-26.21
Tus4-7.2 RH	7.2	5.8	0.95	-26.24
Tus4-7.3 H	7.3	5.5	1.43	-26.39
Tus4-7.5 V	7.5	30.1	25.69	-23.93
Tus4-7.6 V	7.6	10.8	12.07	-24.05
Tus4-7.7 V	7.7	18.5	28.71	-24.20
Tus4-7.9 H	7.9	7.8	1.68	-24.88
Tus4-8.0 V	8.0	19.1	34.38	-24.58
Tus4-8.0 H	8.0	10.5	1.05	-25.02
Tus4-8.3 V	8.3	26.6	40.73	-23.86
Tus4-8.5 V	8.5	22.0	42.30	-23.76
Tus4-8.5 H	8.5	16.2	1.69	-25.57
Tus4-9.0 H	9.0	12.0	0.32	-26.97
Tus4-9.1 V	9.1	47.5	9.75	-24.82
Tus4-9.15 V	9.2	33.3	17.91	-25.27
Tus4-9.25 V	9.3	26.3	36.49	-23.58
Tus4-9.4 V	9.4	14.7	22.13	-24.14

Tus4-9.5 H	9.5	3.6	0.05	-28.99
Tus4-9.6 H	9.6	4.5	0.05	-28.52
Tus4-10.0 H	10.0	-113.1	0.74	-25.43
Tus4-10.5 H	10.5	24.1	0.23	-26.54
Tus4-11.0 H	11.0	12.9	0.17	-26.12
Tus4-11.2 H	11.2	7.7	0.04	-29.45
Tus4-11.2 RH	11.2	5.0	3.66	-26.51
Tus4-11.5 H	11.5	26.3	0.28	-25.29
Tus4-11.8 TV	11.8	24.7	19.54	-23.59
Tus4-11.8 R	11.8	25.8	12.91	-24.06
Tus4-12.0 V	12.0	4.2	65.19	-24.36
Tus4-12.1 H	12.1	3.9	5.89	-25.70
Tus4-12.2 H	12.2	5.7	4.35	-26.09
Tus4-12.3 H	12.3	3.8	1.07	-27.18
Tus4-12.5 H	12.5	3.1	2.10	-25.38
Tus4-12.5 TV	12.5	13.3	49.80	-25.61
Tus4-12.5 TRV	12.5	21.7	24.81	-24.76
Tus4-12.8 TV	12.8	11.3	24.32	-24.14
Tus4-12.8 TRV	12.8	5.3	22.64	-25.01
Tus4-12.9 H	12.9	2.4	2.97	-26.18
Tus4-13.05 V	13.1	9.2	20.64	-24.48
Tus4-13.1 H	13.1	5.1	0.27	-25.49
Tus4-13.3 V	13.3	12.9	15.84	-24.14
Tus4-14.0 H	14.0	2.5	0.04	-27.49
Tus4-14.5 H	14.5	8.2	0.18	-26.28
Tus4-15.0 H	15.0	5.9	0.05	-26.48
Tus4-15.1 H	15.1	9.0	1.07	-26.48
Tus4-15.3 H	15.3	7.8	1.32	-26.84
Tus4-15.5 H	15.5	9.1	0.28	-27.13
Tus4-15.7 H	15.7	8.5	1.34	-26.97
Tus4-16.0 H	16.0	9.6	1.03	-26.30
Tus4-16.1 H	16.1	3.6	4.10	-25.03
Tus4-16.3 H	16.3	14.5	1.76	-26.74
Tus4-16.4 H	16.4	13.3	1.60	-26.73
Tus4-16.5 H	16.5	9.5	0.64	-26.44
Tus4-16.6 RH	16.6	11.0	39.84	-24.53
Tus4-16.7 H	16.7	19.6	6.08	-24.21